Received: 7 December 2020 | Revised: 24 March 2021 | Accepted: 26 March 2021

DOI: 10.1111/bre.12565

RESEARCH ARTICLE

Basin Research | IAS EAGE | WILEY

Effects of basement structures and Carboniferous basin configuration on evaporite distribution and the development of salt structures in Nordkapp Basin, Barents Sea—Part I

Muhammad Hassaan[1,2] | **Jan Inge Faleide**[1,2] | **Roy Helge Gabrielsen**[1] | **Filippos Tsikalas**[1,3]

[1]Department of Geosciences, University of Oslo, Oslo, Norway

[2]Research Centre for Arctic Petroleum Exploration (ARCEx), University of Tromsø, Tromsø, Norway

[3]Vår Energi AS, Stavanger, Norway

Correspondence
Muhammad Hassaan, Department of Geosciences, University of Oslo, Oslo, Norway.
Email: muhammad.hassaan@geo.uio.no

Funding information
Norges Forskningsråd, Grant/Award Number: 228107; Equinor; Vår Energi; Aker BP; Lundin Energy Norway; OMV; Wintershall Dea

Abstract

Potential field data, reprocessed regional 2D seismic reflection profiles and 3D seismic tied to wells were used to study the late Devonian-Permian development of the Nordkapp Basin in Barents Sea. The composite basin can be subdivided into the northeastern, central and southwestern segments that developed above a basement that contains elements of the Timanian and Caledonian regimes. The transition between the Timanian and Caledonian structures is positioned below the central basin segment. The rheological properties, locations, orientations and interaction of inherited structures together with two subsequent extensional phases, defined the presalt rift architecture and gave rise to seven subbasins within Nordkapp Basin. During the late Devonian-early Carboniferous NE-SW oriented extension, the basin consisted of two regional half-grabens (northern and southern) separated by an interbasin ridge. During the late Carboniferous, the shift of extension direction to NW-SE orientation reshaped the two regional half-grabens. In particular, an interbasin transfer zone divided the northern regional half-graben by separating its hinged-margin portion (incipient northeastern segment) from the deeper part (incipient central segment). At the same time, the elevated interbasin ridge separated the incipient central and southwestern segments. Internally within the seven subbasins, the evolving structural elements including cross-cutting master faults and structural highs have influenced the deposition and character of the Pennsylvanian-lower Permian layered evaporite sequence and the distribution of subsequent salt structures. We suggest that the syn-rift to early postrift processes, relative depth of each subbasin, arrangement of the structural highs and depositional palaeo-environment all controlled the thickness and facies of the layered evaporite sequence. The latter in combination with the presalt architecture comprised a laterally varying in thickness and character substratum that during the earliest Triassic influenced the sediment routings and deposition of the progradational system arriving in Nordkapp Basin. The study outcomes are pertinent and applicable to other salt-influenced rift basins worldwide.

KEYWORDS

Barents Sea, layered evaporite sequence, mobile salt volume, Nordkapp Basin, presalt rift geometries, salt structures, structural inheritance

1 | INTRODUCTION

The Nordkapp Basin is a composite, NE-SW-oriented and elongated basin of regional significance in the southwestern Barents Sea. It has a total axial length of ca. 350 km, and its width varies between ca. 25 and 82 km. The Nordkapp Basin has a pronounced dog-leg shape and can be subdivided into three main segments: the northeastern (NENB), the central (CNB) and the southwestern (SWNB; Figure 1; e.g. Gabrielsen et al., 1990; Gernigon et al., 2018; Hassaan et al., 2020; Rojo et al., 2019). It contains thick Pennsylvanian-early Permian layered evaporite sequence (LES) forming salt ridges, walls and stocks of variable sizes, thicknesses and geometries. The LES consists of interbedded halite/salt of mobile property and nonevaporite rocks such as gypsum, anhydrite and carbonates having nonmobile nature, and their relative presence could influence the development of salt structures (Rowan et al., 2019). The stratified LES is documented in Barents Sea, Pyrenees and Betics of Spain, Permian Basin of Europe, South Atlantic, Gulf of Mexico, Levant Basin in eastern Mediterranean, Red Sea and Gulf of Suez, Precaspian Basin, Oman salt basins, Flinders Ranges of Australia, Kuqa Basin of China, La Popa Basin in Mexico, Nova Scotia salt basins and Paradox Basin of the southwestern United States (Rowan et al., 2019 and references therein). The associated top evaporite morphology influences the distribution and thickness of the postsalt Triassic to Cenozoic sequences in the Nordkapp Basin (Rojo et al., 2019). The maximum thickness of the postsalt sedimentary strata in the basin is ca. 9 km (Cedeño et al., 2019; Rojo et al., 2019). Previous studies of the Nordkapp Basin have mainly concentrated on the postsalt evolution steered by salt mobilisation and dynamics alone (e.g. Grimstad, 2016; Koyi et al., 1993, 1995; Nilsen et al., 1995; Rojo & Escalona, 2018; Rowan & Lindsø, 2017), whereas the role of the presalt rift architecture on the internal basin segmentation and on the evaporite accumulation and postsalt evolution has been widely overlooked due to low seismic resolution at depth of the available datasets.

Recently, Hassaan et al. (2021) and Rowan and Lindsø (2017) demonstrated the impact of the presalt rift architecture on the accumulation of the LES, the subsequent passive diapirism and the rejuvenation of salt structures in the Tiddlybanken Basin (Figure 1a). This basin is situated to the southeast of the Nordkapp Basin but has its basin-axis oriented transverse to the Nordkapp Basin and is also much smaller in size. It is still likely that the Tiddlybanken Basin shares some characteristics with the Nordkapp Basin, when the influence from basement structures on its morphology and structuring is concerned (Hassaan et al., 2021). In light of this work, we now investigate in the Nordkapp Basin the deep presalt rift architecture and its impact on the basin evolution, utilising more comprehensive and better resolution datasets than previous studies. The reprocessed and the pseudo-3D seismic datasets used in the present study were made available to academia for the first time. Through structural and stratigraphic interpretations and analyses within the Nordkapp Basin and nearby regions, our aims are to focus on (a) the detailed structural segmentation and deep basin architecture in relation to the inherited regional structures, (b) the synrift to early postrift LES accumulation, (c) the relation between the mapped evaporite volume and presalt basin architecture and (d) the impact of presalt rift architecture and LES on the subsequent basin evolution. The evaporites in the Nordkapp Basin have been a barrier for good data resolution at depth in previous studies, which has been unfortunate because they represent a key substratum for understanding the subsequent basin evolution. Therefore, the present study unravels the deep (presalt) structural configuration of the Nordkapp Basin and links it to the evaporite accumulations and consequent salt structures.

Highlights

- Impact of spatially and rheologically variable inherited structures on basin development revealed in Nordkapp Basin.
- Structural inheritance and two subsequent extensional phases formed seven subbasins within the composite basin.
- Interbasin transfer zones (interbasin antithetic ridge and transfer fault) subdivided the seven subbasins.
- Layered evaporite sequence and salt structures distribution influenced by structural configuration.

2 | GEOLOGICAL SETTING

The basement of the greater Barents Sea was affected by the late Neoproterozoic Timanian orogeny that gave rise to NW-SE trending inherited structures (e.g. Barrère et al., 2009,

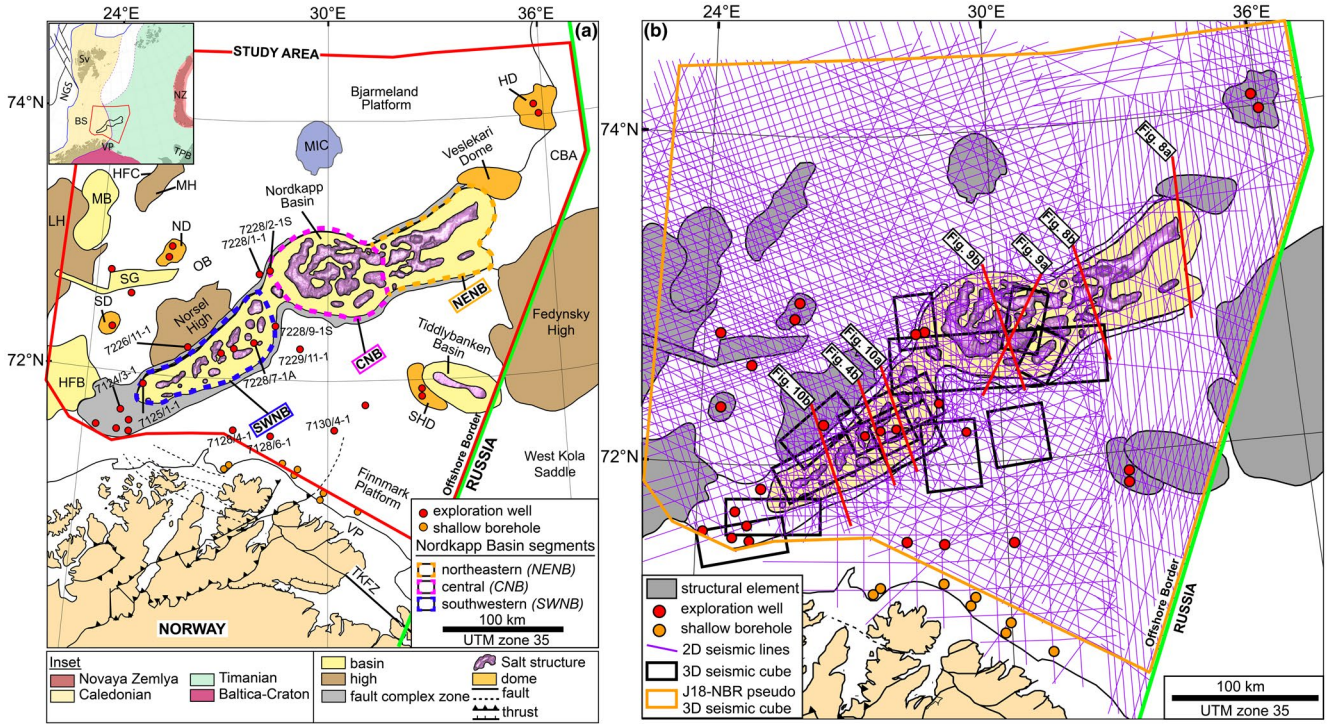

FIGURE 1 (a) Main structural elements of the southwestern and southeastern Norwegian Barents Sea (modified from Hassaan et al., 2020; Mattingsdal et al., 2015) and study area denoted by the red polygon. BS: Barents Sea; CBA: Central Barents Arch; HD: Haapet Dome; HFB: Hammerfest Basin; HFC: Hoop Fault Complex; LH: Loppa High; MB: Maud Basin; MH: Mercurius High; MIC: Mjølnir Impact Crater; ND: Norvarg Dome; NGS: Norwegian-Greenland Sea; OB: Ottar Basin; SD: Samson Dome; SG: Swaen Graben; SHD: Signalhorn Dome; Sv: Svalbard; TPB: Timan-Pechora Basin; VP: Varanger Peninsula; TKFZ: Trollfjorden-Komagelva Fault Zone. (b) Utilised seismic reflection datasets, exploration wells and shallow boreholes, overlaid on the main structural elements. Seismic data courtesy of NPD and TGS [Colour figure can be viewed at wileyonlinelibrary.com]

2011; Faleide et al., 2018; Gabrielsen, 1984; Gee et al., 2006; Pease et al., 2016) and by the Silurian-Devonian Caledonian orogeny that contributed to NE-SW and NNW-SSE trending basement fabric (e.g. Gernigon & Brönner, 2012; Rice et al., 1989; Roberts, 1972; Roberts & Gee, 1985). Several authors have suggested that the late Devonian-Mississippian gravitational/extensional collapse of the offshore part of the Caledonian orogen along inherited NE-SW and NW-SE structures influenced the initiation of the Nordkapp Basin (Breivik et al., 1995; Dengo & Røssland, 1992; Faleide et al., 1993, 2008; Gernigon et al., 2014; Gudlaugsson et al., 1998; Marello et al., 2013; Ritzmann & Faleide, 2007). Recently, Hassaan et al. (2020) inferred that NW-SE trending graben structures mapped in the southeastern Norwegian Barents Sea extend towards the CNB and the SWNB segments of the Nordkapp Basin, following the Timanian inherited structures. It was also suggested that the CNB segment developed due to pre-Mississippian NE-SW extension, whereas the other two segments (NENB and SWNB) resulted from Pennsylvanian NW-SE extension (Gernigon et al., 2018; Hassaan et al., 2020; Rowan & Lindsø, 2017). The Pennsylvanian to early Permian evaporites in the Norwegian Barents Sea were accumulated under warm and arid climate conditions (Larssen et al., 2002), and the LES comprise both mobile (i.e. halite) and nonmobile (i.e. anhydrite) lithologies (Hassaan et al., 2020; Rojo et al., 2019; Rowan & Lindsø, 2017). Cool-water carbonate platform deposits were accumulated at the basin margins due to a shift from arid/warm to temperate depositional environment conditions in the Barents Sea in the middle Permian (Beauchamp, 1994; Stemmerik, 2000).

Triassic sediments from the southeast Urals were accumulated in the Barents Sea during regional subsidence, and by late Triassic the prograding system reached Svalbard, causing deposition of several transgressive-regressive cycles of marine, deltaic and continental clastic sediments (Eide et al., 2018; Glørstad-Clark et al., 2010; Klausen et al., 2015). Several studies suggested that in the Nordkapp Basin, salt diapirism was triggered by early Triassic thick-skinned extension (Jensen & Sørensen, 1992; Koyi et al., 1993, 1995; Nilsen et al., 1995; Rojo et al., 2019; Rojo & Escalona, 2018) and by loading of northwest Triassic progradation of sediments sourced from the Uralides (Dengo & Røssland, 1992; Grimstad, 2016; Rojo et al., 2019; Rowan & Lindsø, 2017). During the Triassic-Jurassic transition, the structural elements in the Barents Sea were slightly reactivated probably due to westward propagating compressional stress from the evolving Novaya Zemlya

fold-and-thrust belt (Hassaan et al., 2020, 2021; Indreværet al., 2018; Müller et al., 2019). Minor subsequent reactivation has been suggested for the middle Jurassic and earliest Cretaceous (Hassaan et al., 2020). However, all structural elements were buried beneath the lower Cretaceous shelf-platform sedimentary complex, which prograded towards south to the southeastern Norwegian Barents Sea (Hassaan et al., 2020, 2021; Midtkandal et al., 2020). On the contrary, other researchers described that the thinning of lower Cretaceous strata towards the salt diapirs was attributed to continued growth due to salt supply from the source layer in the Nordkapp Basin (Koyi et al., 1993, 1995; Rojo & Escalona, 2018) or as gravity-induced contraction (Nilsen et al., 1995). The Carboniferous structures in the southeastern Norwegian Barents Sea were reactivated during the Cenozoic by far-field stress propagating from the Eurekan orogeny taken place farther to the northwest (Gabrielsen et al., 1997; Gac et al., 2020; Hassaan et al., 2020). In the Nordkapp Basin, most of the late Cretaceous to Cenozoic strata have been eroded due to late Cenozoic uplift and related preglacial and Plio-Pleistocene glacial erosion episodes (Baig et al., 2016; Henriksen et al., 2011; Lasabuda, Laberg, Knutsen, & Høgseth, et al., 2018; Lasabuda, Laberg, Knutsen, & Safronova, 2018; Rojo et al., 2019; Tsikalas et al., 2012, 2021).

3 | DATA AND METHODS

The magnetic anomaly map from Gernigon et al. (2018) was integrated with the reprocessed seismic data to get better control on the presalt structural interpretation and basement configuration. Furthermore, filtered gravity data were also incorporated to confirm the locations of the salt structures and to compare them with the 3D salt model based on the multi-z seismic interpretation (Figure 2). The seismic database consists of conventional 2D multichannel seismic (MCS) reflection profiles, twelve 3D seismic data surveys and a newly synthetically constructed pseudo-3D seismic cube (J18-NBR-3D) covering an area of 51,500 km^2 over the entire Nordkapp Basin, the Norsel High and the Veslekari Dome (Figures 1 and 2 and Table 1a). An additional 95,400-km^2 region in the surrounding of the three mentioned structural elements has been interpreted in order to understand the regional tectonics and basinal context of the southeastern and southwestern Norwegian Barents Sea that is relevant for the Nordkapp Basin evolution. The J18-NBR-3D seismic cube was constructed by TGS by utilising all available 2D multichannel NBR seismic datasets in the Barents Sea, whilst a subset was created covering the study area (Figure 1b). The twelve 3D seismic data surveys (Table 1a) have been utilised to interpret the salt structures and postsalt key horizons with precision. The 2D MCS profiles in the same area are part of several regional surveys with an average line spacing of 3–5 km (Figure 1b and Table 1a). The quality of the NBR06 to NBR14, NPD-BA-11, BARE02, BARE05 and IS-CNBE-06 seismic surveys in the NENB and SWNB segments is fairly good for the mapping of postsalt horizons. However, in the CNB segment the seismic quality depreciates drastically due to the presence of complex salt structures including overhangs, as well as steep dips adjacent to the diapirs. The reprocessed BSSE14-RE, CFI-NBR and IS-CNB-01 seismic surveys have excellent seismic quality and are mainly utilised for the presalt interpretation, including the base-salt seismic horizon, layered evaporites and rift geometries (Table 1b). The BSSE14RE

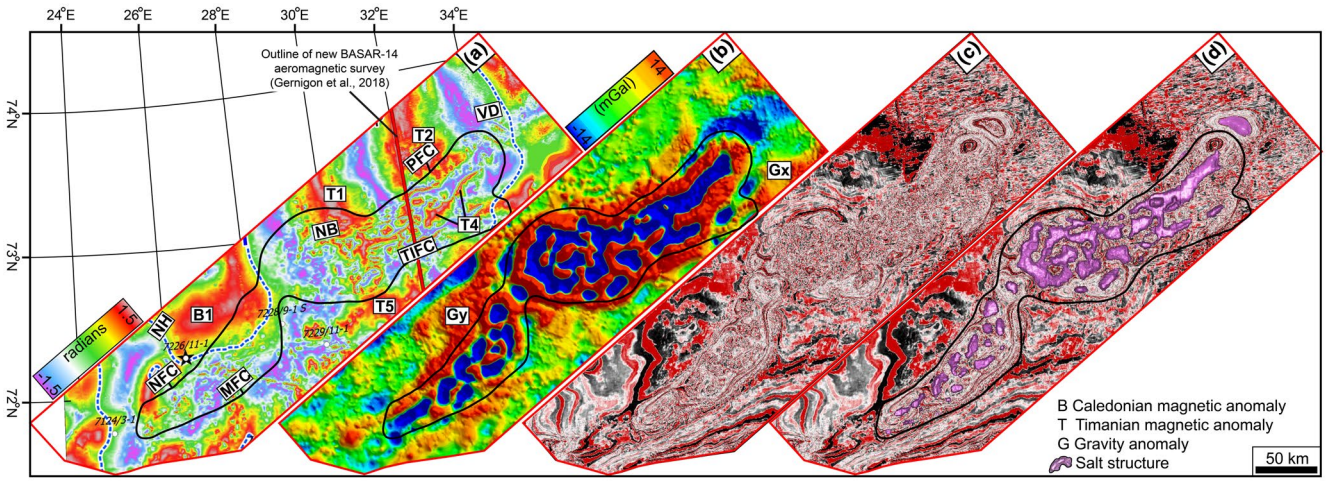

FIGURE 2 Illustrative comparison between various utilised datasets: (a) magnetic data (radians; Gernigon et al., 2018), (b) gravity data (mGal; high-pass filter cut-off 30 km, data courtesy of TGS), (c) uninterpreted J18-NBR-3D seismic data pseudo-cube (time slice at 2-s twt), (d) interpreted salt structures within J18-NBR-3D seismic data pseudo-cube (time slice at 2-s twt). MFC: Måsøy Fault Complex; NFC: Nysleppen Fault Complex; NB: Nordkapp Basin; NH: Norsel High; PFC: Polstjerna Fault Complex; TIFC: Thor Iversen Fault Complex; VD: Veslekari Dome [Colour figure can be viewed at wileyonlinelibrary.com]

TABLE 1A Utilised seismic reflection datasets (twt: two-way travel time, s)

Survey	3D/2D	Year	Acquisition company/ authority	Record time (twt, s)	Study area coverage (3D/km^2, 2D/km)	Resolution
J18-NBR-3D	Pseudo-3D	2018	TGS	6	ca. 146,900	Very good/excellent
NKFE11	3D	2011	TGS	7	ca. 5,937	Very good/excellent
BG0804	3D	2008	BG Group	5	ca. 652	Very good/excellent
ED16001	3D	2016	Edison Norge	6	ca. 1,514	Good
MC3D	3D	2003	WesternGeco/TGS	4.5	ca. 1,056	Good
SH9102	3D	2010	Norsk Shell	5	ca. 569	Moderate
ST309	3D	2004	Equinor	6.5	ca. 1,954	Good
ST0624	3D	2008	Equinor	12	ca. 836	Moderate
ST0811	3D	2010	Equinor	7.4	ca. 1,077	Good
ST0828	3D	2009	Equinor	4.2	ca. 1,061	Very good/excellent
ST9403	3D	2002	Equinor	5.4	ca. 1,036	Very good/excellent
ST10011	3D	2010	Equinor	6.5	ca. 2,466	Moderate
ST10012	3D	2011	Equinor	4.5	ca. 667	Very good/excellent
BSSE14RE	2D	2014	NPD/TGS	9	ca. 18,305	Very good/excellent
CFI-NBR	2D	2018	TGS	10	ca. 28,270	Very good/excellent
NPD-BA-11	2D	2011	NPD	9	ca. 18,305	Moderate
IS-CNB-01	2D	2001	Inseis AS	8	ca. 2,966	Very good/excellent
IS-CNBE-06	2D	2006	Inseis AS	9.8	ca. 535	Good
NBR06	2D	2006	NPD	10	ca. 4,245	Moderate
NBR07	2D	2007	NPD	10	ca. 4,560	Moderate
NBR08	2D	2008	NPD	10	ca. 9,330	Moderate
NBR09	2D	2009	NPD	10	ca. 4,650	Moderate
NBR10	2D	2010	NPD	10	ca. 2,690	Moderate
NBR12	2D	2012	NPD	10	ca. 9,825	Good
NBR14	2D	2014	NPD	6	ca. 7,200	Moderate
BARE02	2D	2002	NPD/TGS	6	ca. 4,785	Poor
BARE05	2D	2005	NPD	6	ca. 2,405	Poor

TABLE 1B Calculated vertical seismic resolution for the reprocessed BSSE14RE and CFI-NBR surveys that are particularly utilised for presalt interpretation

Zone		Frequency (Hz) (F)	Interval velocity (m/s) (V)	Wavelength (m) (λ = V/F)	Vertical resolution (m) (λ/4)
Shallow	Cretaceous to Jurassic	50	2,335	47	12
Intermediate	Triassic	30	4,000	133	33
Deep	Permian to Pennsylvanian	15	6,280	419	105
		20	6,280	314	79
	Mississippian	15	4,960	331	83
		20	4,960	248	62

and CFI-NBR surveys were reprocessed by TGS in 2014 and 2018, respectively, utilising a processing sequence that included amongst other: bandwidth enhancement, multiple elimination using linear transforms, Tau-p deconvolution, premigration conditioning, Kirchhoff prestack time migration, anisotropy analysis and radon demultiple. Finally, all available seismic surveys have been used for the postsalt interpretation.

Eleven exploration wells located in the vicinity of the study area have been utilised together with shallow stratigraphic

boreholes (Bugge et al., 1995) on the southern part of the east Finnmark Platform (Figure 1). The well data were utilised to establish well-to-seismic ties (Figure 3), time-to-depth conversion functions and the seismostratigraphic framework for the seismic interpretation in the study area. Formation tops from the wells were used for the subdivision of the upper Palaeozoic to Cenozoic successions. Eleven seismic sequences bounded by 12 seismic horizons were mapped to subdivide the upper Palaeozoic to Cenozoic strata and used to establish the lithostratigraphic and chronostratigraphic sequences (Figure 3 and Table 2). It should be noted that the reflections dated to the base of the Carboniferous (BCa?) and the top of the Serpukhovian (TS) are noncontinuous. Data resolution depreciates somehow below the LES of the Gipsdalen Group (Figure 3 and Table 2), whereas the postsalt seismic reflections mostly are continuous and easily resolved. Selected seismic sections from the excellent resolution reprocessed CFI-NBR and BSSE14RE seismic surveys (Table 1a) were used for the detailed structural and stratigraphic analyses. The salt structures were interpreted in three dimensions using the multi-z interpretation tool (Petrel v.2019, Schlumberger), whilst the J18-NBR-3D pseudo-3D seismic cube was the main input for the creation of the 3D salt model (Figures 1b, 4 and 5). The present-day volume of the mobile salt in the Nordkapp Basin was calculated using the constructed three-dimensional salt model, whilst minor loss of the volume due to Cenozoic uplift/erosion and dissolution processes is not included (Move v.2019.1, Petroleum Experts; Figures 4 and 5). The further subdivision of the evaporites into mobile and nonmobile parts and presalt rift strata was based on seismic facies analysis (Table 2).

4 | BASIN ANATOMY AND STRUCTURAL VARIATIONS

The Nordkapp Basin is a long-lived NE-SW oriented depocenter that evolved over a transitional inherited basement and was influenced by presalt extension, LES accumulation, salt mobilisation and salt structure rejuvenation processes during the late Devonian to the Cenozoic. In this section, we describe the potential field (magnetic and gravity) data that show the considerable basement topography, the highly variable base-salt structural relief based on the seismic data and the distribution of salt structures, along with present-day evacuated salt volume estimates in the different Nordkapp Basin segments (NENB, CNB and SWNB). Together with the formal naming of the first-order structural elements for the area (Norwegian Petroleum Directorate/NPD Gabrielsen et al., 1990; Mattingsdal et al., 2015), in the following sections, we also use informal naming and extensive abbreviations that help us to describe all mapped detailed features

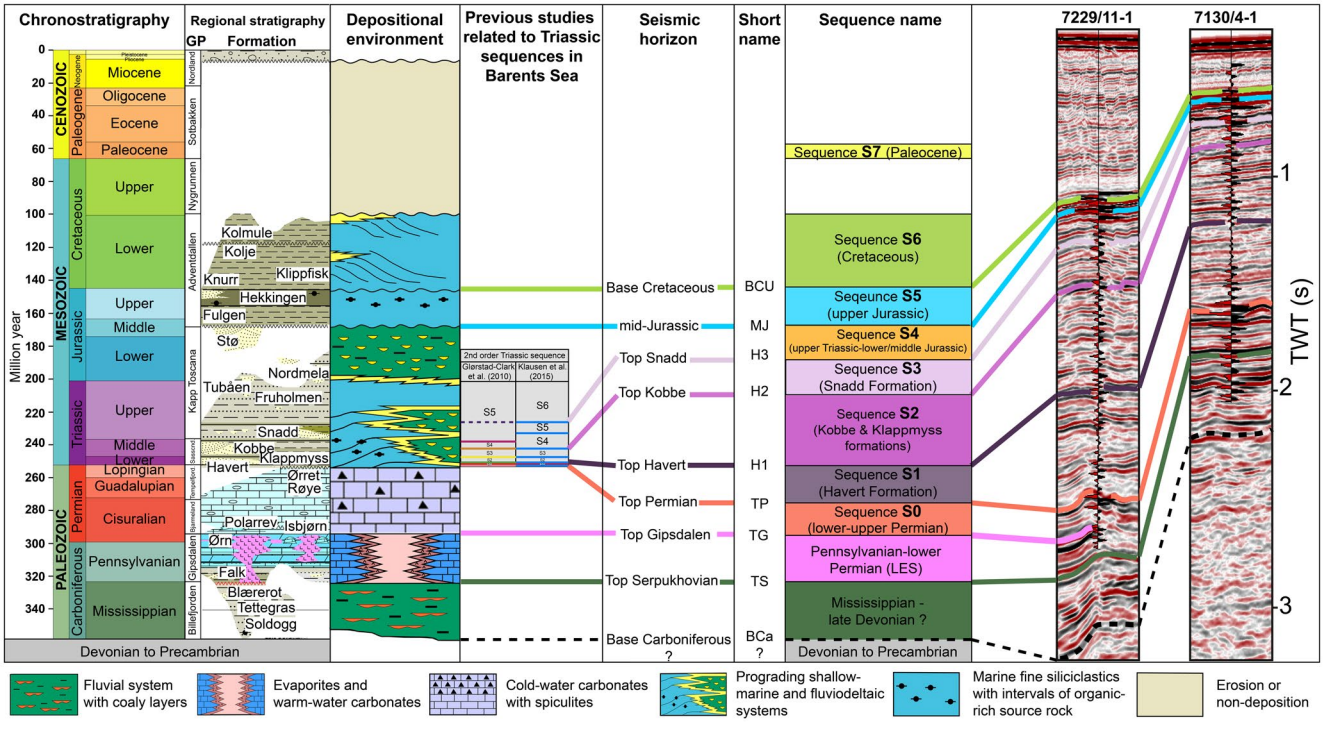

FIGURE 3 Stratigraphic framework and key seismic horizons interpreted throughout the study area based on 11 exploration wells (Figure 1a,b). Regional stratigraphy and depositional environment scheme is based on Larssen et al. (2002) modified after Gernigon et al. (2018) and Rojo et al. (2019) and geologic timescale after Gradstein and Ogg (2020). GP: (stratigraphic) group. The seismic-stratigraphic framework is also tied to earlier chrono-stratigraphic schemes for Triassic successions by Glørstad-Clark et al. (2010) and Klausen et al. (2015). TWT, two-way travel time, s [Colour figure can be viewed at wileyonlinelibrary.com]

TABLE 2 Interpreted seismic facies (SF) and core data from selected wells

Seismic facies (SF)	Description
SF1	Horizontal to inclined, semicontinuous, subparallel to diverging and medium- to high-amplitude seismic reflections, characterised as clastic infill, that is, sandstone, shale and coal, of the Billefjorden Group of Mississippian age (Figure 3) in the graben structures and on the platform or hinged margins. The reflections become chaotic beneath the salt structures
SF2	Semicontinuous to continuous, parallel to subparallel and medium to strong amplitude seismic reflections interpreted as interbedded, mixed nonhalite and nonmobile lithologies, that is, anhydrite, gypsum of the Gipsdalen Group of Pennsylvanian to early Permian age (Figure 3)
SF3	Featureless and chaotic seismic reflections, occasionally delimited at top and base by high amplitude and continuous reflections that laterally converge and pinch out, characterised as mobile halite lithology of the Gipsdalen Group of Pennsylvanian to early Permian age (Figure 3)

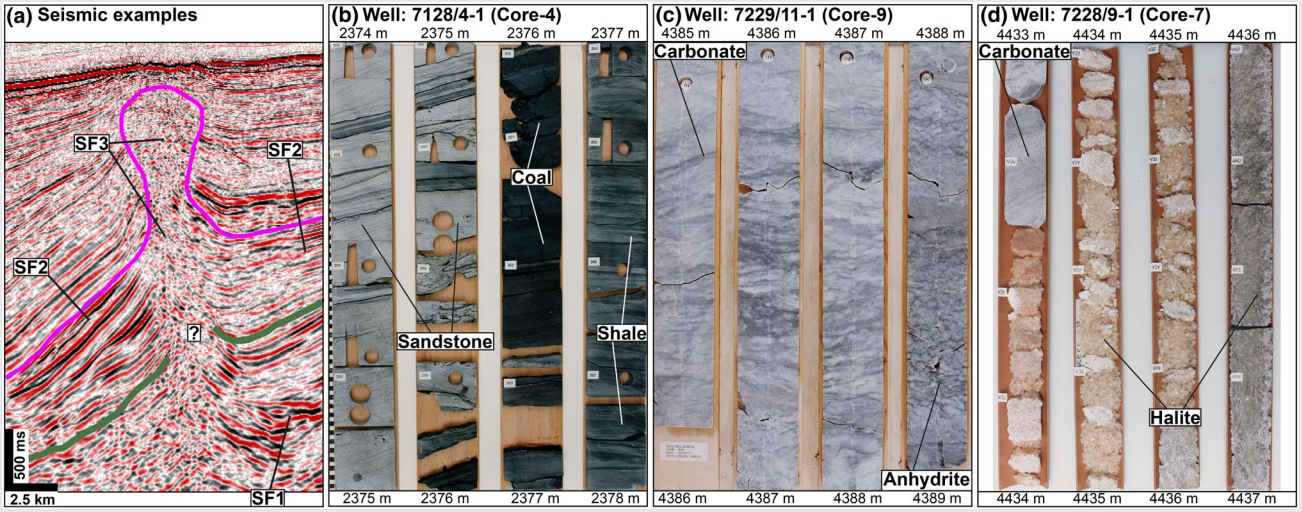

in the study (Figure 6). The basin is bounded by fault complexes (i.e. Polstjerna, Thor Iversen, Nysleppen and Måsøy) and is dissected by internal cross-cut thick-skinned master faults (i.e. M1–M14) and transfer zones (i.e. northern and southern). The northern and southern transfer zones represent a transfer fault and an antithetic interbasin ridge, respectively (sensu Gawthorpe & Hurst, 1993). The Nordkapp Basin is further subdivided into seven subbasins (SB1–SB7; Figure 6). The characteristics of the salt structures, that is, shape, lateral extent, structural type and orientation are also presented in Table 3. We informally named the most prominent, branched and complex salt structure in the CNB segment as 'Dragon foot (DF) salt structure' (Figure 5 inset). The DF salt structure consists of several connected walls with different orientations. The present-day average thickness of the evacuated salt from the LES is calculated for each subbasin as the cumulative volume of mobile salt divided by the area of the subbasin (Figure 4). The present-day estimated volume of each salt structure is added accordingly to the respective subbasin, that is, SB1–SB7, where the corresponding salt structure is present (Figures 5a and 6c; Table 4). The calculated mobile salt thickness is based on the present-day three-dimensional structural geometry of the salt structures (Figure 4c,d). However, minor volume loss due to Cenozoic uplift/erosion and dissolution processes is not included in the current calculations along with the residual nonmobile evaporites (Figure 5c).

4.1 | Basement inherited structures and regional structural configuration

The potential field (magnetic and gravity) data show that the surroundings of the Nordkapp Basin possess a considerable basement topography and complex basinal configuration (Figure 7). The contrasting Timanian and Caledonian deformational regimes can be separated in space. It is possible to identify assumed zones of weakness that likely promoted basin initiation in later events of extension phases in the Nordkapp Basin (Figures 2a,b and 7). On the Finnmark Platform, the magnetic data exhibit arch-shaped anomalies that we attribute to the Caledonian nappes of the Middle Allochthon basement and are ascribed as structural lineations (Gernigon et al., 2018). These arches swing from NE-SW on the onshore Varanger Peninsula to NW-SE in the offshore domain and cut through the CNB segment and the Bjarmeland Platform (Figure 7a). The thrust units of the so-called Middle Allochthon Front (MAF) signify a major tectonic boundary

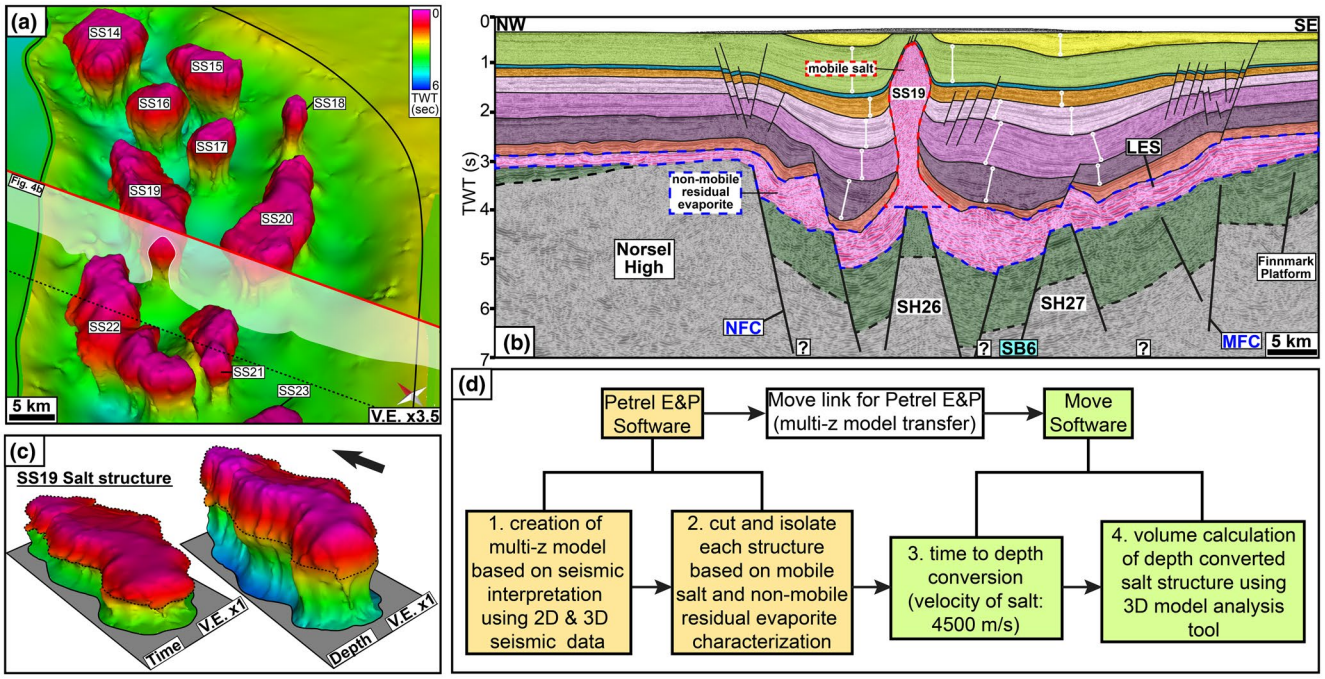

FIGURE 4 (a) Three-dimensional (3D) view of the multi-z salt model (time-structure; TWT: two-way travel time, s) at top Gipsdalen level displays scattered salt structures in the southwestern segment (SWNB) of the Nordkapp Basin. (b) Interpreted seismic section (TWT: two-way travel time, s; vertical exaggeration: 5×) illustrating presalt geometries, layered evaporite sequence (LES), salt structures and postsalt sedimentation patterns in the southwestern segment (SWNB). MFC: Måsøy Fault Complex; NFC: Nysleppen Fault Complex; SB: Subbasin. Colour rasters correspond to interpreted sequences in Figure 3. Open white circles connected by white lines display the thickness variations. (c) Depth conversion of the isolated SS19 salt structure from the multi-z model of the Nordkapp Basin. (d) Utilised method for present-day volume estimation of the salt structures. V.E: Vertical exaggeration. Structural highs (SH) are annotated as in Figure 6b and salt structures (SS) as in Figure 5a. Profile location shown also in Figures 1b and 6a. Seismic data courtesy of NPD and TGS [Colour figure can be viewed at wileyonlinelibrary.com]

onshore mainland Norway and separate the Caledonian from the Timanian inherited structures, continuing offshore in the Barents Sea (Figure 7a; Gernigon et al., 2018; Hassaan et al., 2020 and references therein).

The northeastern tip of the NENB segment terminates sharply at the prominent central Barents Sea magnetic domain (CBSM; Figure 7a; Gernigon et al., 2018). The northern part of the CBSM includes the Haapet and Veslekari domes, whilst the southern part bounds the Fedynsky High. A series of prominent magnetic anomalies (T1–T5) in the Timanian domain also affect the platform areas that surround the Nordkapp Basin. In particular, the NENB segment terminates against magnetic anomaly T2 that impacts the Polstjerna Fault Complex to the west (Figure 7a). It is also obvious that a sharp NW-SE trending magnetic low affects the NE-SW oriented T4 magnetic anomaly in the centre of the NENB segment. Towards the Bjarmeland Platform, the Polstjerna Fault Complex terminates against the T1 magnetic anomaly. Farther south-southeast, the boundary of the T1 magnetic anomaly is delineated by the SW-dipping M4 extensional fault (Figures 6c and 7a).

The CNB segment seems to comprise the most complex region of the Nordkapp Basin, probably due to the fact that the MAF cuts through its centre and separates the Caledonian from the Timanian domains beneath it. Towards the Finnmark Platform, the CNB segment is constrained by the T5 magnetic anomaly within the Timanian domain, and this anomaly extends farther east beneath the Signalhorn Dome (Figure 7a). A prominent magnetic low characterises the Caledonian domain outside the CNB segment towards the Bjarmeland Platform. However, inside the CNB segment, the magnetic anomalies are blurred due to the interference with the complex salt structures. Towards the Finnmark Platform, the NW-SE trending magnetic lineations, that are parallel to the MAF, approach the CNB segment and terminate against the M8 extensional fault (Figure 6c). The M8 fault seems to coincide with the envisaged prolongation of the southern boundary of the T5 magnetic anomaly (Figures 6c and 7a).

A series of magnetic anomalies that broadly define the regional structural configuration of the basement in the Nordkapp Basin and its vicinity were identified. The positive B1 and B2 magnetic anomalies suggest the existence of two deep and NNW-SSE trending Palaeozoic basement highs related to the Caledonian inherited structures (Gernigon & Brönner, 2012; Gernigon et al., 2014), whereas anomaly B0 is identified in the current study beneath the newly identified basin X4 (Figure 7a). Four deep basins X1-4

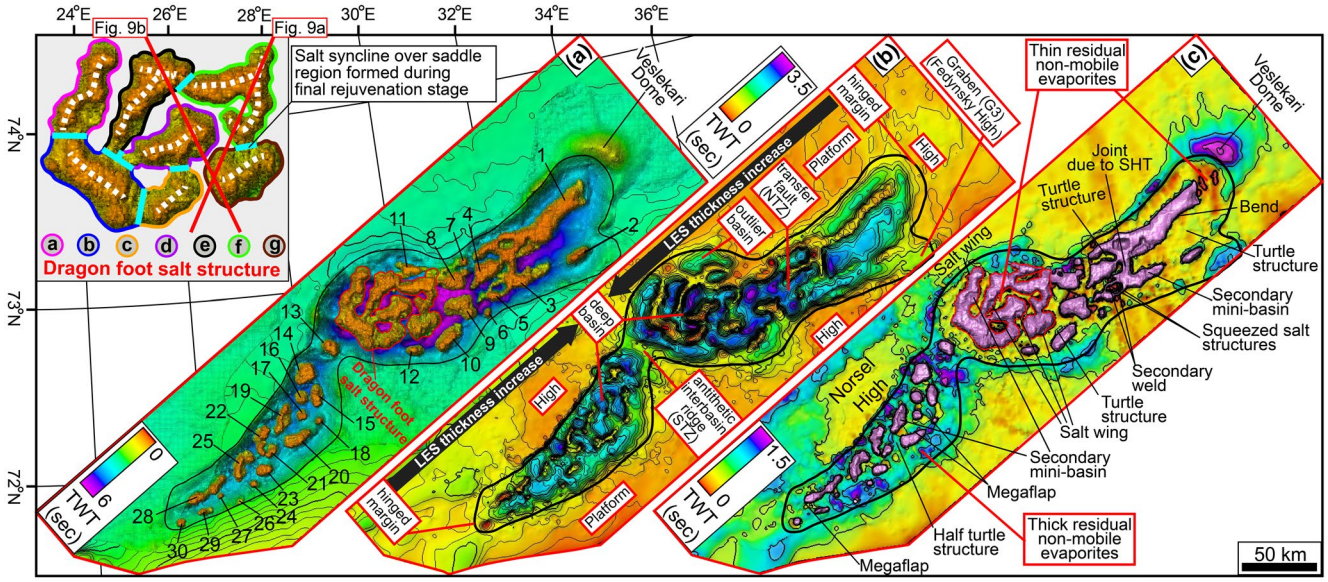

FIGURE 5 (a) Multi-z salt model (time-structure; TWT: two-way travel time, s) at top Gipsdalen level illustrating the complex arrangement of the salt structures in the Nordkapp Basin. Numbers refer to the salt structures (SS) described in the text. The estimated present-day evacuated salt volume from the LES and structural characteristics of the individual salt structures are presented in Table 3. Inset: zoom-in of the DF salt structure showing its different segments (a–g). SHT: Structural high Timanian. (b) Time thickness map (TWT: two-way travel time, s) between the base-salt (top Serpukhovian) and regional level (based on Bjarmeland and Finnmark platforms) shows Pennsylvanian-early Permian LES accumulations controlled by presalt rift architecture before the salt mobilisation. (c) Time thickness map (TWT: two-way travel time, s) between the base-salt (top Serpukhovian) and top-salt (top Gipsdalen) displays salt evacuation from the Pennsylvanian-early Permian LES, salt structures and residual nonmobile evaporites in the different segments of the Nordkapp Basin [Colour figure can be viewed at wileyonlinelibrary.com]

are interpreted towards the west of the CNB segment. The NE-SW trending X1-2 Carboniferous basins seem to be the prolongations of the Ottar Basin with absence of evaporites (Figure 1a). The nature and sediment infill of the X3-4 basins is unknown (Figure 7a, black stippled lines). The SWNB segment is restricted by the positive B1 magnetic anomaly that is part of the Norsel High magnetic domain (NHM; Figure 7a). The B1 anomaly further appears to affect the Nysleppen Fault Complex, which is the hard-linked boundary between the Norsel High and the SWNB segment. On the Finnmark Platform, the magnetic lineations curve along with the MAF and converge towards the SWNB segment, whilst they terminate against the segmented Måsøy Fault Complex (Figure 7a). The magnetic lineations parallel to the MAF are cut by the NW-SE oriented lineaments that coincide with the M12–14 faults. The southwestern limit of the SWNB segment is marked by a prominent magnetic low (Figure 7a).

The NENB, CNB and SWNB segments are all characterised by regional NE-SW oriented negative gravity anomalies, and internally, the present-day salt structures influence the observed gravity anomalies as it is evident by their structural outline imprints (Figures 2b and 7b). The connection between the NENB and CNB segments appears continuous, whereas a prominent positive gravity anomaly separates the CNB and SWNB segments (Figure 7b). Generally, positive gravity anomalies bound the Nordkapp Basin. One prominent gravity anomaly, named Gx, is located on the northeastern tip of the Nordkapp Basin beneath the Fedynsky High and covers the eastern side of the NENB segment. The thick evaporites of the Veslekari Dome interfere with the gravity anomaly of the Gx-structure, resulting in a gravity low at the northeastern tip of the Nordkapp Basin (Figure 7b). In the Fedynsky High, a gravity low follows the graben G3 that is connected with the NENB segment. On the Finnmark Platform, the gravity highs are curved along the MAF and converge towards the CNB segment. Another prominent gravity anomaly, named Gy, is located west of the SWNB segment and beneath the Norsel High (Figure 7b).

4.2 | Structural segmentation and Carboniferous rift architecture

The base-salt structural relief which corresponds to the Mississippian (top Serpukhovian) level is highly variable at the different Nordkapp Basin segments (NENB, CNB and SWNB). The rift architecture comprises elongated fault-bounded structural highs and marginal master faults that controlled the accumulation of evaporites in isolated depocenters. The structural configuration of the base-salt relief is most complex in the CNB, in comparison to the NENB and SWNB segments (Figure 6). The CNB is a circular basin as defined on the top Permian and BCU levels, and it was previously described to exhibit symmetric and full-graben geometry that developed

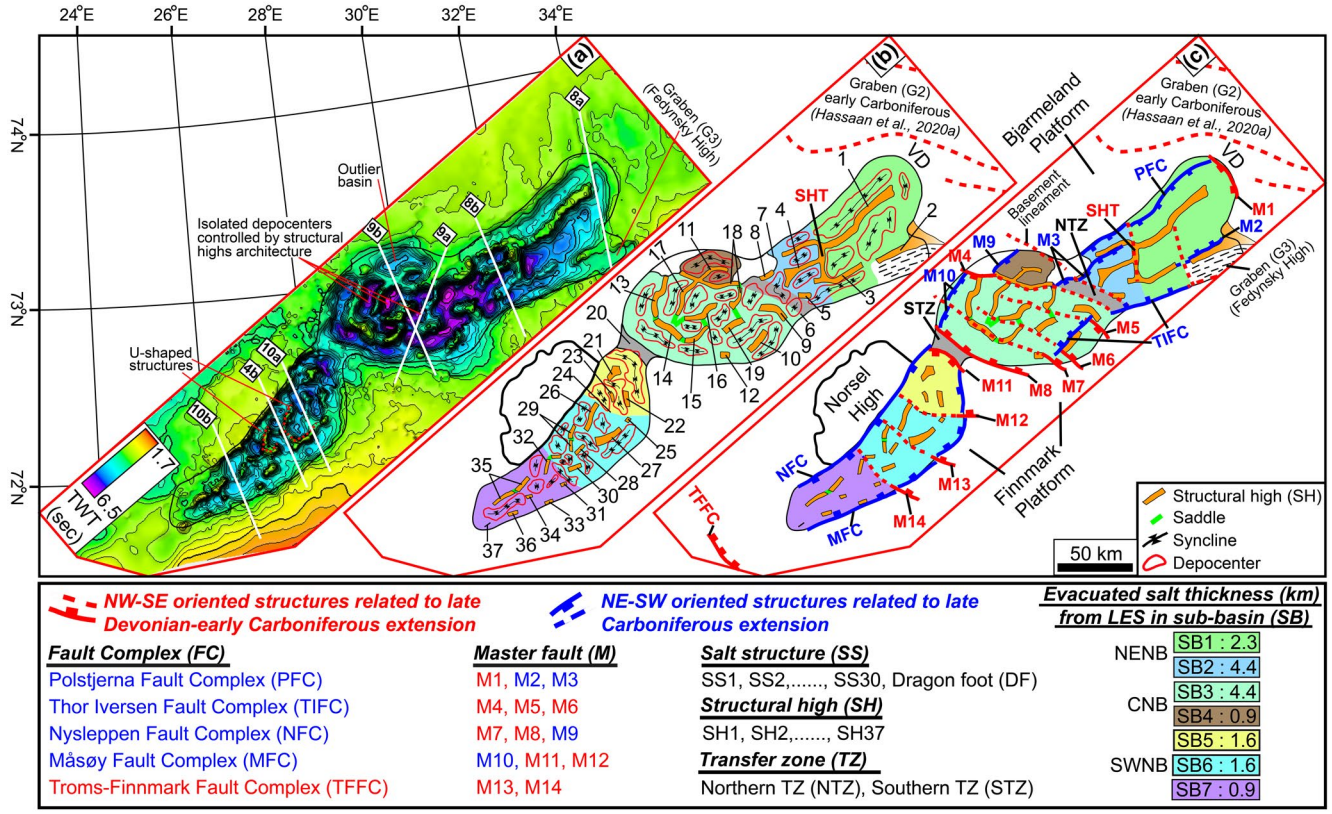

FIGURE 6 (a) Top Serpukhovian (TS) time-structure map displaying the base-salt structural relief, together with location of seismic profiles in the corresponding figures (TWT: two-way travel time, s); (b) second-order basinal and structural configuration, numbers refer to structural highs, SH, and associated salt structures, SS (in Figure 5a); and (c) master faults and structural highs arrangement. Subbasins SB1–7 are illustrated with different colour rasters. Abbreviations refer to structural features shown in the legend and described in the text. Present-day estimated average evacuated salt thickness (km) from the layered evaporite sequence (LES) is given in the subbasin legend [Colour figure can be viewed at wileyonlinelibrary.com]

during pre-Mississippian NNE-SSW extension (Gernigon et al., 2018; Rowan & Lindsø, 2017). Similarly, the NENB and SWNB segments were viewed as elongated depocenters at the Permian and BCU levels and were defined as asymmetric half-grabens formed during Pennsylvanian NW-SE extension (Gernigon et al., 2018; Rowan & Lindsø, 2017). However, the internal rift architecture in the Nordkapp Basin is more complex as it will become evident from the descriptions in the following sections where we utilise a series of maps and sections to illustrate detailed structural observations.

4.2.1 | Northeastern Nordkapp Basin segment

The northernmost limit of the NENB segment is delineated by the SW-dipping M1 normal fault (Figure 6c). At base Carboniferous BCa? level, the M1 fault defines the southern boundary of the horst that separates the NW-SE oriented graben G2 (Hassaan et al., 2020) beneath the Veslekari Dome and the NENB segment (Figure 6c). The SE-dipping normal Polstjerna Fault Complex is the structure that separates the NENB segment and the Bjarmeland Platform towards the west (Mattingsdal et al., 2015). The Polstjerna Fault Complex terminates against the M1 fault to the northeast (Figures 6 and 8). The influence of the Polstjerna Fault Complex minimises towards the southwest where it dies out against a NW-SE basement lineament, SHT (Figure 6). The presalt and postsalt components of the Polstjerna Fault Complex are decoupled by the observed salt pillow (Figure 8). In the south, the Thor Iversen Fault Complex bounds the NENB segment from the Finnmark Platform. The Thor Iversen Fault Complex is a NNW-dipping thick-skinned extensional fault (Gabrielsen et al., 1990). Towards the northeast, the normal throw of the Thor Iversen Fault Complex decreases and it is connected to the southern boundary fault of the graben G3 (defined by Hassaan et al., 2020) that stretches below the Fedynsky High and dips towards NW (Figures 6c and 7a). Towards southwest, the Thor Iversen Fault Complex extends into the CNB segment and is cross-cut by the NW-SE striking normal faults M4–M7 (Figure 6c).

The NENB segment is further subdivided into two subbasins, SB1 and SB2, by the NW-SE oriented structural high SHT (Figure 6c). Towards the northeast, subbasin SB1 forms a hinged-margin relationship with the NW-SE oriented horst and dies out against the M1 fault (Figure 6). The NNW-dipping

TABLE 3 Present-day volume estimates and structural characteristics of the salt structures in the three Nordkapp Basin segments: northeastern (NENB), central (CNB) and southwestern (SWNB)

Salt structure (SS)	Present-day volume (km^3)	Shape of salt structure	Lateral extent (km)		Axial ratio	Type of salt structure	Orientation
			Length	Width			
a. Northeastern Nordkapp segment (NENB)							
1	ca. 7,759	Elongated	ca. 81	ca. 13.2 (SW), ca. 10.4 (NE)	6.86	Wall	NE-SW
2	ca. 436	Elongated	ca. 14.4	ca. 4.6	3.13	Wall	NE-SW
3	ca. 2,355	Elongated	ca. 27.7	ca. 7.6	3.64	Wall	NE-SW
4	ca. 1674	Elongated	ca. 24.7	ca. 8.6	2.87	Wall	NE-SW
5	ca. 517	Subcircular	ca. 8.5	ca. 5.2	1.63	Stock	
6	ca. 135	Circular	ca. 5.1	ca. 3.3	1.55	Stock	
7	ca. 152	Circular	ca. 5	ca. 4.9	1.02	Stock	
Total volume	ca. 13,028						
b. Central Nordkapp segment (CNB)							
8	ca. 1,070	Subcircular	ca. 17.6	ca. 16.3	1.08	Stock	
9	ca. 1,675	Subcircular	ca. 17.2	ca. 13.6	1.26	Stock	
10	ca. 1,133	Elongated	ca. 20.5	ca. 7.6	2.70	Wall	NE-SW
11	ca. 479	Elongated	ca. 14.3	ca. 6.8	2.10	Wall	E-W
12	ca. 288	Subcircular	ca. 10.1	ca. 5.5	1.84	Stock	
Dragon foot (DF)	**a**: ca. 1,955 **b**: ca. 2,840 **c**: ca. 1,253 **d**: ca. 2,272 **e**: ca. 2,362 **f**: ca. 2,916 **g**: ca. 2,074	Branched	**a**: ca. 26.6 **b**: ca. 27.6 **c**: ca. 19.3 **d**: ca. 24.9 **e**: ca. 33.4 **f**: 23.2 (E-W) + 20.4 (NE-SW) = ca. 43.6 **g**: ca. 19.9	**a**: ca. 9.8 **b**: ca. 11.6 **c**: ca. 7.1 **d**: ca. 8.1 **e**: ca. 8.6 **f**: ca. 7.4 **g**: ca. 13.3	**a**: 2.71 **b**: 2,38 **c**: 2.72 **d**: 3.07 **e**: 3.88 **f**: 5.89 **g**: 1.50	Connected salt walls and stock	**a**: NNE-SSW **b**: NW-SE **c**: NE-SW **d**: NE-SW **e**: NNE-SSW **f**: E-W to NE-SW **g**: NE-SW
13	ca. 394	Subcircular	ca. 11.2	ca. 6.9	1.62	stock	
Total volume	ca. 20,746						
c. Southwestern Nordkapp segment (SWNB)							
14	ca. 879	Subcircular	ca. 12.1	ca. 8.5	1.42	Stock	
15	ca. 522	Elongated	ca. 11.4	ca. 4.1	2.78	Wall	N-S
16	ca. 396	Subcircular	ca. 5.7	ca. 4.9	1.16	Stock	
17	ca. 210	Subcircular	ca. 5.2	ca. 4.7	1.11	Stock	
18	ca. 56	Circular	ca. 4.4	ca. 3.1	1.42	Stock	
19	ca. 754	Elongated	ca. 20.1	ca. 4.2	4.79	Wall	NE-SW
20	ca. 602	Elongated and elliptical	ca. 17.6	ca. 4.2	4.19	Wall	NE-SW
21	ca. 179	Subcircular	ca. 8.7	ca. 5.1	1.71	Stock	
22	ca. 638	Elongated	ca. 18.6	ca. 3.8	4.89	Wall	N-S
23	ca. 298	Elongated	ca. 9.7	ca. 5.8	1.67	Stock	ENE-WSW
24	ca. 59	Subcircular	ca. 4.3	ca. 4.0	1.08	Stock	
25	ca. 847	Elongated and elliptical-L	17.8 (N-S) + 9.9 (E-W) = ca. 27.7	ca. 5	5.54	Wall	N-S to E-W

(Continues)

TABLE 3 (Continued)

26	ca. 41	Subcircular	ca. 2.7	ca. 2.4	1.13	Stock	
27	ca. 10	Subcircular	ca. 3.1	ca. 2.6	1.19	Stock	
28	ca. 546	Elongated	ca. 27.8	ca. 4.6	6.04	Wall	NE-SW
29	ca. 90	Elongated	ca. 9.1	ca. 3.1	2.94	Wall	NE-SW
30	ca. 65	Subcircular	ca. 5.2	ca. 4.6	1.13	Stock	
Total volume	ca. 6,192						

TABLE 4 Estimated average evacuated salt thickness from the layered evaporite sequence (LES) in the different subbasin parts (SB1–7) of the Nordkapp Basin

Subbasin (SB)	Salt structure (SS)	Present-day volume (km^3)	Area (km^2)	Average evacuated salt thickness (volume/area) (km)
SB1	3/4 SS1 and SS2-3	ca. 8,611	ca. 3,646	ca. 2.3
SB2	1/4 SS1 and SS4-7	ca. 4,417	ca. 983	ca. 4.4
SB3	SS8-10, Dragon Foot, SS12-13	ca. 20,267	ca. 4,614	ca. 4.4
SB4	11	ca. 479	ca. 533	ca. 0.9
SB5	SS14-17	ca. 2,007	ca. 1,255	ca. 1.6
SB6	SS18-23 and 1/3 SS25	ca. 2,809	ca. 1,876	ca. 1.5
SB7	SS24, 2/3 SS25 and SS 26-30	ca. 1,376	ca. 1,581	ca. 0.9

M2 normal fault marks the western boundary of the SH2 structural high (Figures 6c and 8). The SH2 structural high separates subbasin SB1 from the full-graben G3 that stretches beneath the Fedynsky High. Graben G3 terminates against a NW-SE lineament, whilst the SH1 structural high shows a slight bend at the junction with the same lineament (Figure 6c). Subbasin SB2 defines a transition region between the main NENB and CNB segments and exhibits complex structures (Figure 8b). It is noteworthy that a thick-skinned reverse fault that dips NNW connects with the secondary weld in the postsalt sediments and is reaching the seafloor (Figure 8b). At the margins of the NENB and within subbasin SB1 clastic infill seismic facies (Table 2; SF1: Billefjorden Group of Mississippian age) can be identified with moderate confidence, whilst the quality of seismic data depreciates drastically in the deeper parts of subbasin SB2 (Figure 8).

4.2.2 | Central Nordkapp Basin segment

The S-dipping M4 normal fault marks the possible boundary between the CNB and NENB segments (Figures 6c and 9). The continuation of the Thor Iversen Fault Complex separates the CNB segment from the Bjarmeland Platform towards the east. The M8 normal fault dips NNE and marks the southwestern boundary of the CNB segment (Figures 6c and 9a). The M9 and M10 SE-dipping normal faults bound the CNB segment from the Bjarmeland Platform towards the west (Figure 6c). An antithetic interbasin ridge bounded by the NW-SE striking M8 and M11 faults separates the CNB from the SWNB segment (Figure 6c).

Internally, the CNB segment includes subbasins SB3 and SB4. Subbasin SB3 consists of several structural highs with different trends and is much larger and deeper than subbasin SB4 (Figure 6). The M5-7 normal faults strike E-W and interfere with the structural highs in the CNB segment. In particular, the M5 normal fault dips to SSW and the M6-7 faults dip towards NNE, and the complex array of structural highs creates isolated depocenters of evaporite accumulations (Figure 6b,c). The same structural highs (SH13 to SH19) are also responsible for the development of the most prominent, branched and complex 'DF salt structure' that consists of several connected walls in the Nordkapp Basin (Figure 5a; Table 3). The NW-SE striking M5-7 normal faults cross-cut the structural highs and create saddles (Figure 6b,c). Moreover, subbasin SB4 is a shallow outlier basin bounded by fault M9 to the west and is restricted by the SH18 structural high to the southwest (Figures 6c and 9b). At the margins of the CNB segment and within subbasin SB4, clastic infill seismic facies (Table 2; SF1: Billefjorden Group of Mississippian age) can be identified with moderate confidence. However, it is not possible to identify the same seismic facies (SF1) in the central and deepest parts of subbasin SB3 as the quality of seismic data depreciates significantly (Figure 9a and Table 2).

4.2.3 | Southwestern Nordkapp segment

The SW-dipping M11 normal fault and the NE-dipping Troms–Finnmark Fault Complex (TFFC) form the northeastern and southwestern boundaries of the SWNB segment, respectively. The SE-dipping Nysleppen Fault Complex separates

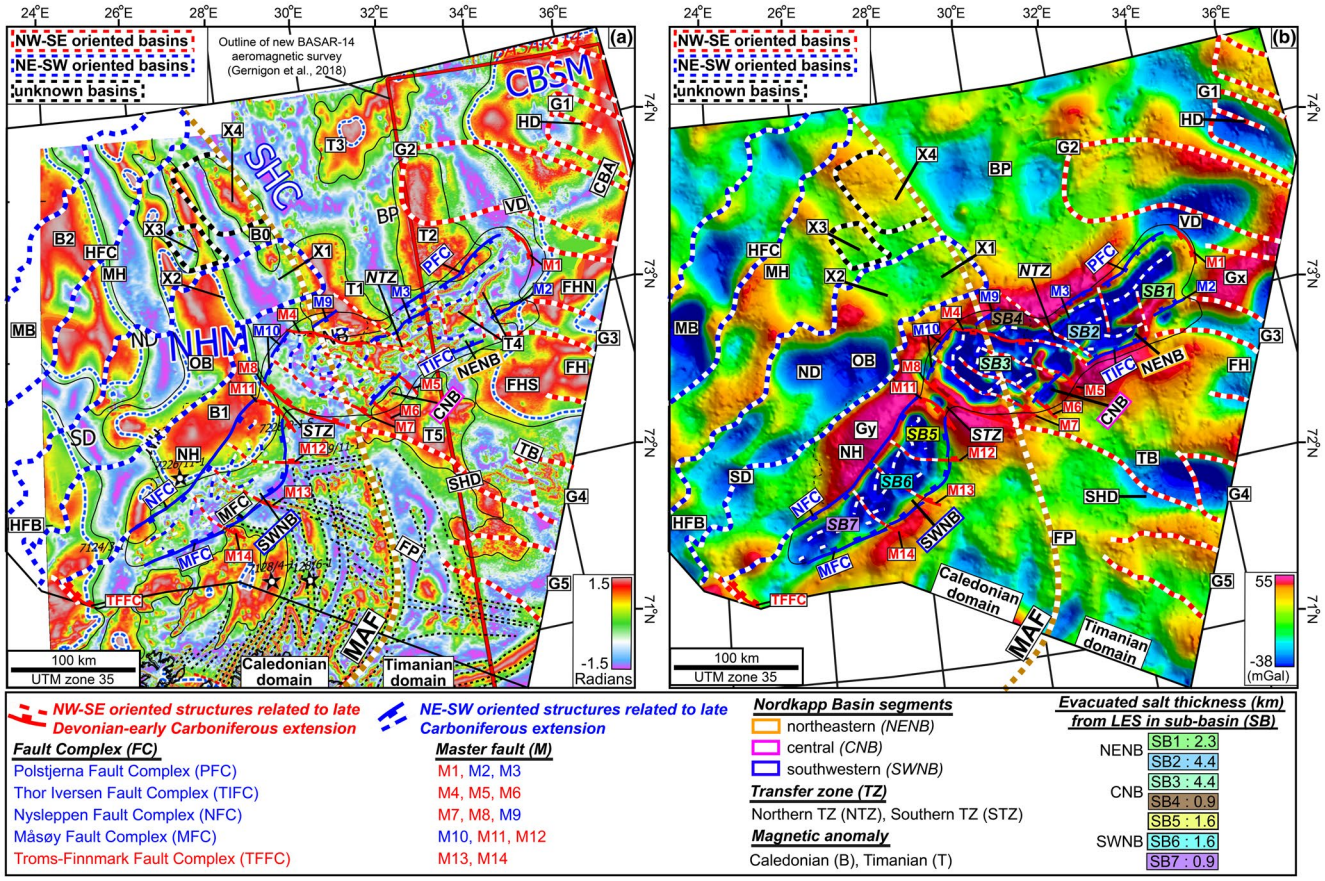

FIGURE 7 (a) Tilt derivative of the total magnetic field map (Gernigon et al., 2018) and (b) gravity map high-pass filtered with cut-off 100 km (data courtesy of TGS) overlaid with the structural configuration based on seismic interpretation in the southeastern and southwestern Barents Sea. X1-4: newly interpreted/inferred basins (see text for details). The utilised abbreviations (followed by number or letter) denote: B: Caledonian magnetic anomaly; G: Graben; Gx: Gravity anomaly x; Gy: Gravity anomaly y; T: Timanian magnetic anomaly. BP: Bjarmeland Platform; CBSM: central Barents Sea magnetic domain; FH: Fedynsky High; FHN: Fedynsky High north; FHS: Fedynsky High south; FP: Finnmark Platform; MAF: Middle Allochthon Front; NB: Nordkapp Basin; NH: Norsel High; SHC: Scott Hansen Complex magnetic low domain; TB: Tiddlybanken Basin; VD: Veslekari Dome. Other abbreviations as in Figure 1a [Colour figure can be viewed at wileyonlinelibrary.com]

the SWNB segment from the Norsel High towards the west (Figures 6c and 10). The Nysleppen Fault Complex is an extensional feature and may represent a fundamental basement lineament that is composed of several faults with significant dip-slip (Gabrielsen et al., 1990). Moreover, the segmented W-dipping Måsøy Fault Complex separates the SWNB segment from the Finnmark Platform (Figure 6c). The Nysleppen and Måsøy fault complexes are thick-skinned extensional features that were primarily active during late Carboniferous to early Permian (Gabrielsen et al., 1990; Figure 10). In several places, the Pennsylvanian to early Permian LES decouples the presalt thick-skinned part of the Nysleppen and Måsøy fault complexes from postsalt faults at the western and eastern margin of the SWNB segment, respectively. The southern limits of both the Nysleppen and Måsøy fault complexes terminate against the NW-SE trending faults following probably the Troms–Finnmark Fault Complex (Figure 6c).

Internally, the NE-dipping M12 and M14 normal faults divide the SWNB into subbasins, SB5–7 (Figures 6b,c and 10). A similar fault, M13, cross-cuts the structural highs in subbasin SB6 (Figure 6c). Subbasin SB5 consists of structural highs that curve along the margin of the SWNB segment (Figure 6b,c). Subbasin SB6 consists of several structural highs, forming two U-shaped structural features that strike NE-SW and are separated by the M13 fault (Figure 6a). In subbasin SB7, the structural highs strike NE-SW and are surrounded by shallow depocenters in contrast to subbasins SB5 and SB6 (Figure 6a). Clastic infill seismic facies (Table 2; SF1: Billefjorden Group of Mississippian age) can be interpreted in the SWNB segment with greater confidence due to shallower depth in comparison to the NENB and CNB segments (Figure 10; Table 2).

4.3 | Evaporite deposition and the distribution of salt structures

The NENB, CNB and SWNB segments of the Nordkapp Basin contain salt structures (SS) that are associated with

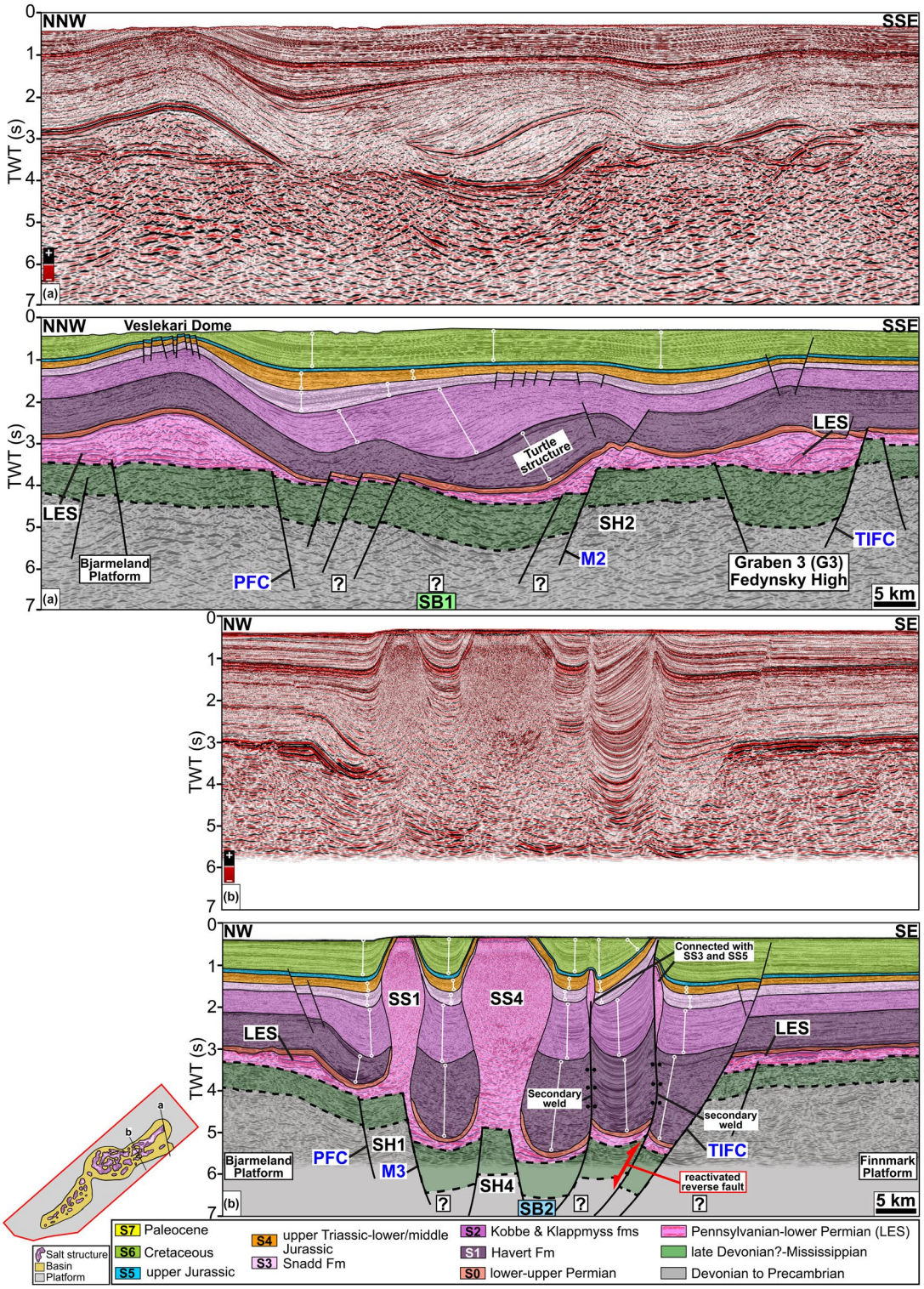

FIGURE 8 (a, b) Un-interpreted and interpreted seismic sections (TWT: two-way travel time, s; vertical exaggeration: 5×) illustrating presalt geometries, layered evaporite sequence (LES), salt structures and postsalt sedimentation patterns in the northeastern segment (NENB) of the Nordkapp Basin. M: Master fault; PFC: Polstjerna Fault Complex; TIFC: Thor Iversen Fault Complex; SB: Subbasin. Colour rasters correspond to interpreted sequences in Figure 3. Open white circles connected by white lines display the thickness variations. Structural highs (SH) are annotated as in Figure 6b and salt structures (SS) as in Figure 5a. Present-day volume estimates are presented in Table 3a. Profile locations in Figures 1b and 6a. Seismic data courtesy of NPD and TGS [Colour figure can be viewed at wileyonlinelibrary.com]

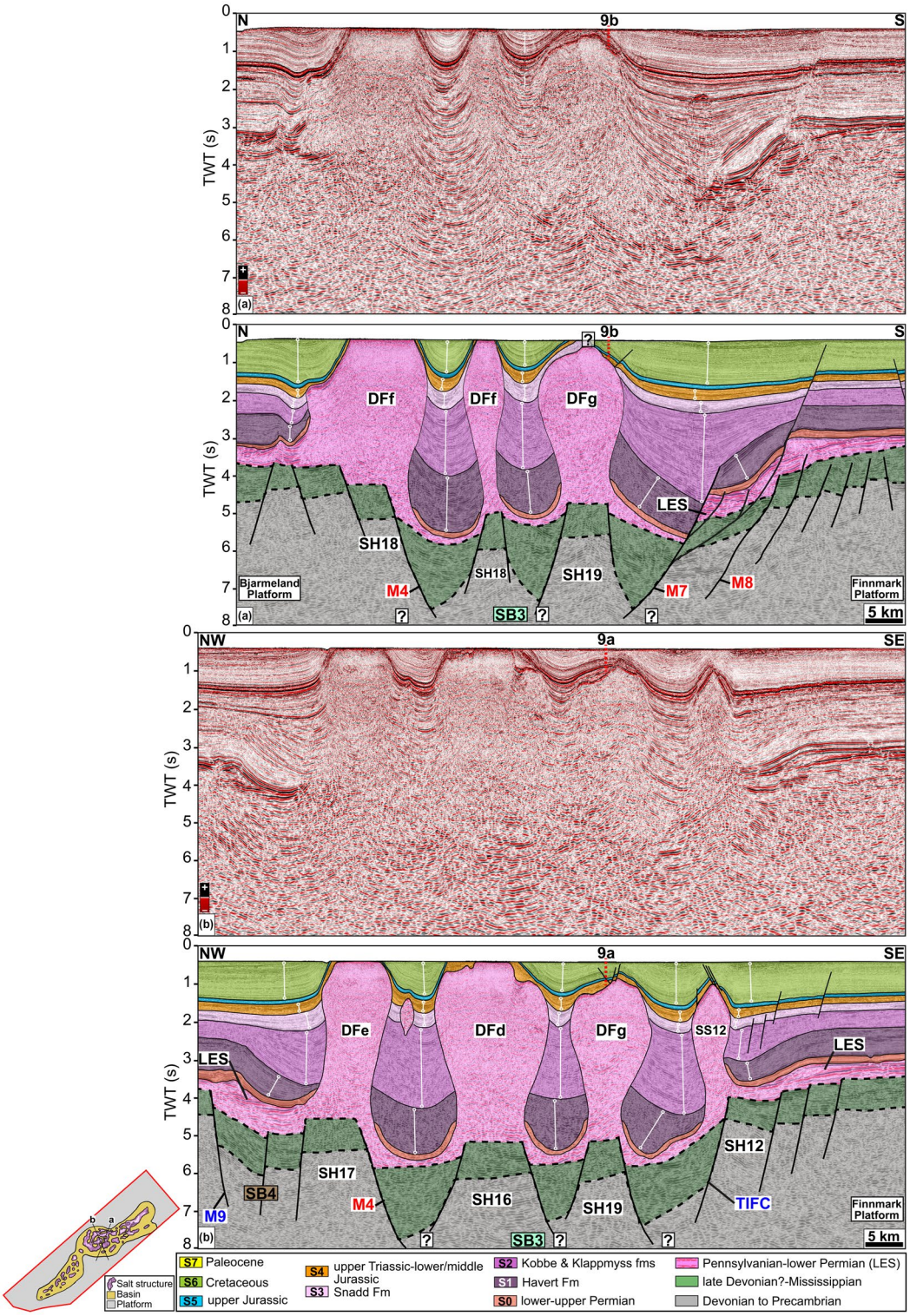

FIGURE 9 (a, b) Uninterpreted and interpreted seismic sections (TWT: two-way travel time, s; vertical exaggeration: 5×) illustrating presalt geometries, layered evaporite sequence (LES), salt structures and postsalt sedimentation patterns in the central segment (CNB) of the Nordkapp Basin. DF: Dragon foot; M: Master fault; SB: Subbasin; TIFC: Thor Iversen Fault Complex. Colour rasters correspond to interpreted sequences in Figure 3. Open white circles connected by white lines display the thickness variations. Structural highs (SH) are annotated as in Figure 6b and salt structures (SS) as in Figure 5a. Present-day volume estimates are presented in Table 3b. Profile locations in Figures 1b and 6a. Seismic data courtesy of NPD and TGS [Colour figure can be viewed at wileyonlinelibrary.com]

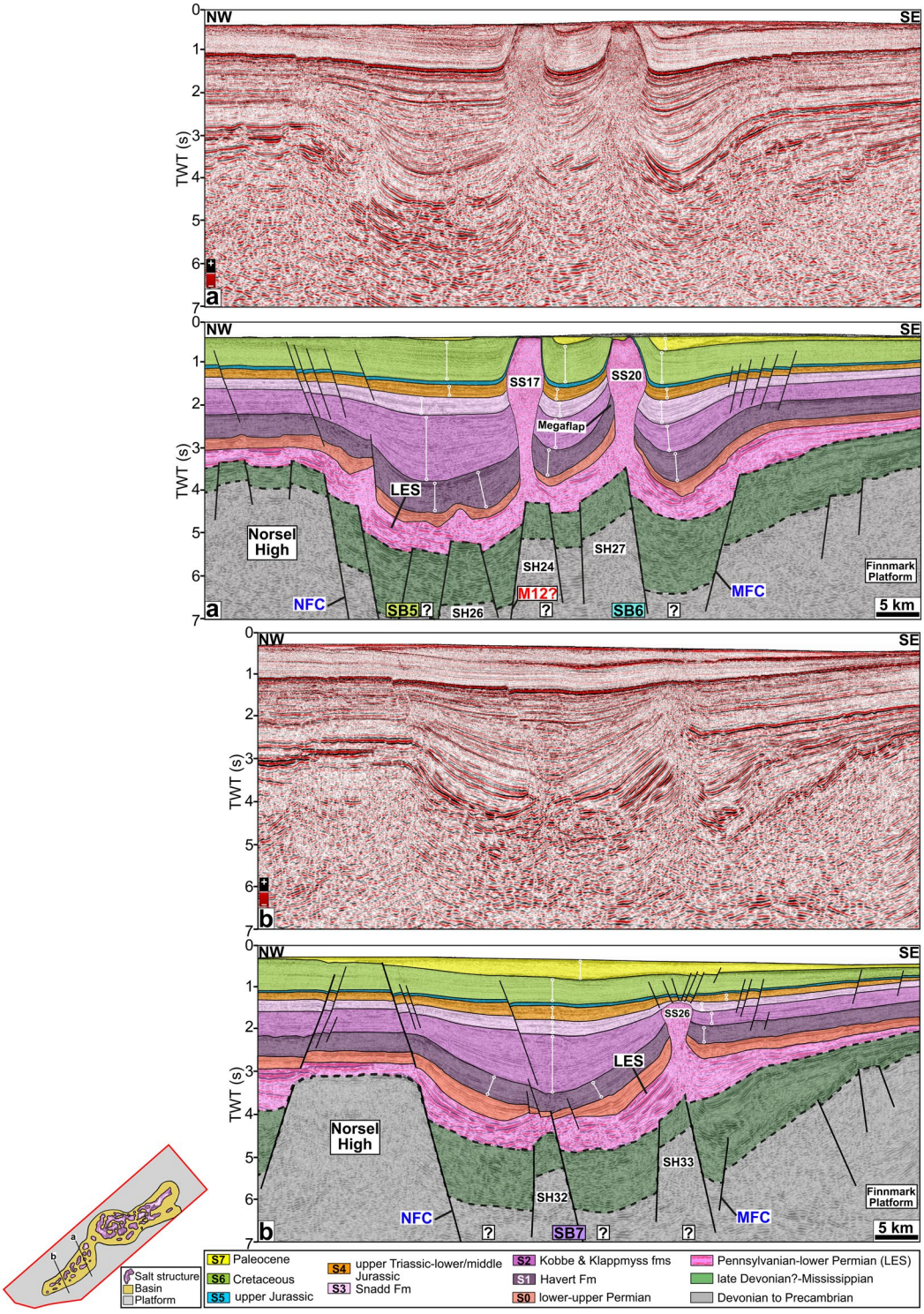

FIGURE 10 (a, b) Un-interpreted and interpreted seismic sections (TWT: two-way travel time, s; vertical exaggeration: 5×) illustrating presalt geometries, layered evaporite sequence (LES), salt structures and postsalt sedimentation patterns in the southwestern segment (SWNB) of the Nordkapp Basin. NFC: Nysleppen Fault Complex; MFC: Måsøy Fault Complex; SB: Subbasin. Colour rasters correspond to interpreted sequences in Figure 3. Open white circles connected by white lines display the thickness variations. Structural highs (SH) are annotated as in Figure 6b and salt structures (SS) as in Figure 5a. Present-day volume estimates are presented in Table 3c. Profile locations in Figures 1b and 6a. Seismic data courtesy of NPD and TGS [Colour figure can be viewed at wileyonlinelibrary.com]

distinct postsalt structural styles, including turtle structures, secondary welds, collided mini-basins, salt wings and megaflaps (Figure 5c). The interpreted salt structures show different sizes, shapes, orientations and lateral extent that were influenced by the late Permian to Cenozoic postsalt sedimentation in the Nordkapp Basin (Figures 5 and 8–10;

Table 3). The salt structures were sourced from the LES (SF2, Table 2a) that can be identified with precision at the basin marginal pillow structures and within the SWNB segment. However, due to data quality depreciation, it is not possible to classify the individual layers of the LES within the salt structures or beneath the deep mini-basins (Hassaan et al., 2021). The presence of numerous large salt structures show that the CNB segment contains a thicker unit of mobile salt evacuated from the LES in comparison to the NENB and SWNB segments (Figure 5; Table 3). Accordingly, the remnant LES is thin in the CNB and NENB segments. In contrast, the SWNB segment contains less mobile salt and thick residual LES (Figures 5c and 8–10; Table 3).

Overall, the NENB segment comprises seven salt structures SS1–7, including one of the longest (SS1: ca. 81 km) NE-SW trending salt walls of the Nordkapp Basin (Figures 5a and 8b; Table 3). The SS1 salt wall widens towards the southwest (ca. 13.2 km) near the structural high SHT in comparison to the northeast (ca. 10.3 km; Figure 5c and Table 3). SS1 displays a prominent bend approximately in the middle of the structure (map view) and joins with the SS3 salt wall over the NW-SE trending structural high SHT (Figures 5c, 6c and 8b). Subbasin SB1 contains an estimated present-day volume of ca. 8,611 km^3 and an average thickness of ca. 2.3 km of prediapiric evacuated salt from the LES (Table 4). Subbasin SB2 contains an estimated present-day volume of ca. 4,417 km^3 and an average evacuated salt thickness of ca. 4.4 km from the LES (Figures 5c and 6c; Table 4). The two squeezed salt structures are connected with the SS3 towards northeast and with SS5 to the southwest (Figures 5c and 8b). The mini-basins around the squeezed salt structure collide and display two secondary welds. The thick-skinned reverse fault that connects with the secondary weld reached to the seafloor and has pushed up the entire mini-basin (Figure 8b).

The CNB segment comprises seven salt structures, including the most complex and voluminous 'DF' salt structure that is branched and consists of several connected walls (Figure 5c). The SB3 subbasin includes salt structures SS8–10, DF and SS12–13 with a cumulative salt volume of ca. 20,267 km^3 and an average thickness of evacuated salt thickness of ca. 4.4 km from the LES (Figure 5; Tables 3 and 4). The DF salt structure is the most prominent feature of subbasin SB3, and the scattered deep-seated structural highs (that based on our detailed interpretation we exclude the possibility of being velocity pull-up artefacts beneath the salt structures) define the orientation of the various segments (Figure 5b; Table 3). The SS13 is predominantly sourced from subbasin SB3 and partially from subbasin SB5. The shallow outlier subbasin SB4 contains the SS11 salt structure with an estimated present-day volume of 479 km^3 and average evacuated salt thickness of ca. 0.9 km from the LES (Figure 5c; Tables 3 and 4).

The SWNB segment contains 17 salt structures SS14–30 (Figure 5a and Table 3). Subbasin SB5 consists of salt structures SS14–17 with estimated present-day salt volume of ca. 2,007 km^3 and average evacuated salt thickness of ca. 1.6 km from the LES (Figures 5c and 10a; Tables 3 and 4). Subbasin SB6 contains the salt structures SS18–23 and one-third of SS25 with an estimated salt volume of ca. 2,809 km^3 and evacuated salt thickness of ca. 1.5 km from the LES (Figure 5a; Tables 3 and 4). The SS25 salt structure is situated at the boundary between subbasins SB6 and SB7, and the mobile salt volume of it is therefore added according to the ratio of the structure present in both subbasins (Figures 5c and 6). Subbasin SB7 contains the entire SS24, two thirds of SS25 and the entire SS26–30 salt structures with an estimated salt volume of ca. 1,376 km^3 and salt thickness of ca. 0.9 km from the LES (Figure 5; Tables 3 and 4).

5 | DISCUSSION

5.1 | Basement structural topography and its influence on basin development

The prominent CBSM magnetic anomaly pattern is related to the Timanian inherited structures and restricts the northeastern limit of the Nordkapp Basin (Figures 7a and 11b). The western extension of the CBSM lineament in the area along the northern part of the Fedynsky High (FHN, Fedynsky High north) swings to become parallel with the G3 Carboniferous graben so that it provides the structural high associated with the SS2 salt structure (Figures 8a and 11). We therefore conclude that the thick-skinned Thor Iversen Fault Complex is controlled by the thick and rheologically strong crust of the CBSM that separates the Fedynsky High from the NENB segment to the east (Figures 8b and 11b; Gernigon et al., 2018). To the west, the southern edge associated with magnetic anomaly T2 has influenced the thick-skinned Polstjerna Fault Complex along the NW boundary of the NENB segment. Internally, the deep Timanian structure associated with the T2 magnetic signature seems to control the NW-SE oriented SHT structural high that is the boundary between subbasins SB1 and SB2 (Figures 6c and 11b). Towards the Bjarmeland Platform, the NW-SE trending magnetic anomaly T1 is related to the rheologically strong crust of the Timanian inherited structures that lie beneath subbasin SB4 (Figure 11b). This could explain why subbasin SB4 is relatively shallow, contains thinner evaporites and is less affected by the subsequent extension in comparison to subbasin SB3 (Figures 6, 9b and 11b). We accordingly suggest that the M4 is a thick-skinned boundary fault that is controlled by the Timanian structure (T1 anomaly) and is mainly responsible for the evolution of subbasin SB3 (Figure 11b). Towards the

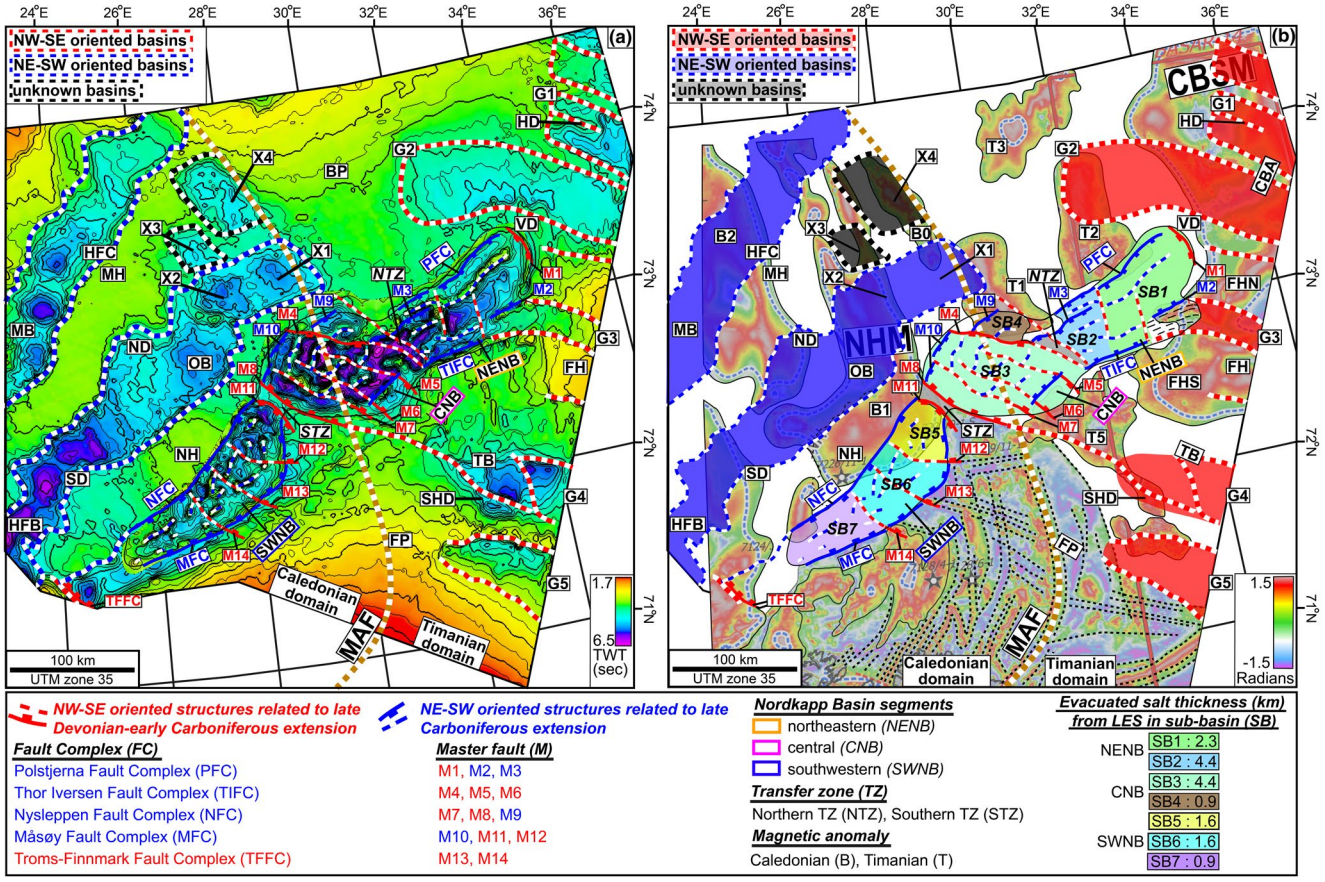

FIGURE 11 (a) Time-structure (TWT: two-way travel time, s) map at the Top Serpukhovian (TS) level for the Nordkapp Basin and base Carboniferous (BCa?) level for the surrounding region illustrating the regional structural configuration and (b) prominent magnetic anomalies from the magnetic tilt derivative data overlaid with the structural configuration based on seismic interpretation in the southeastern and southwestern Barents Sea. Subbasins SB1–7 are illustrated with different colour rasters within the Nordkapp Basin. X1-4: newly interpreted/inferred basins (see text for details). The utilised abbreviations (followed by number or letter) denote: B: Caledonian magnetic anomaly; G: Graben; T: Timanian magnetic anomaly. BP: Bjarmeland Platform; CBSM: central Barents Sea magnetic domain; FH: Fedynsky High; FHN: Fedynsky High north; FHS: Fedynsky High south; FP: Finnmark Platform; MAF: Middle Allochthon Front; NB: Nordkapp Basin; NH: Norsel High; NHM: Norsel High magnetic domain; TB: Tiddlybanken Basin; VD: Veslekari Dome. Other abbreviations as in Figure 1a [Colour figure can be viewed at wileyonlinelibrary.com]

Finnmark Platform, the prominent Timanian structure (T5 anomaly) creates a platform between the NW-SE oriented graben G4 related to Tiddlybanken Basin and the CNB segment (Figure 11; Hassaan et al., 2020). Recently, Hassaan et al. (2021) suggested a basement-involved, arcuate horst related to the pre-existing Timanian basement grain that could be the prolongation of the deep structure represented by the T5 magnetic anomaly and corresponding lineation towards the southeast (Figure 11b).

The suggested location of MAF separates the deep Timanian structures from the Caledonian ones and cuts through the CNB segment (Figure 11b). On the Finnmark Platform, the curved arches and parallel lineations to the MAF display the orientation of the deep Caledonian nappes (Gernigon et al., 2018 and references therein). The overprint of the Caledonian nappes on the NW-SE oriented Timanian structures created a deep and complex structural division within the CNB segment. Within the Caledonian domain of the CNB segment, the orientations of the shallow structures (Figures 7 and 11, red stippled lines), including the basin boundary fault M8, are oblique to the magnetic low that is parallel to the MAF and extend northwards into the Bjarmeland Platform. The oblique nature of the shallow structures reveals a strong control of the older Timanian inherited structures within the Caledonian domain (Figure 11a). Farther to the west, the basin boundary fault M11 is controlled by the deep structure represented by the B1 magnetic anomaly. However, the prolongation of the deep Palaeozoic structural high associated with the Norsel High magnetic domain gives rise to the distinct antithetic interbasin ridge between the CNB and SWNB segments (Figures 11a and 12). The presence of magnetic anomaly B1 could also explain why the Norsel High is less affected by later extension. The cross-cutting NW-SE magnetic

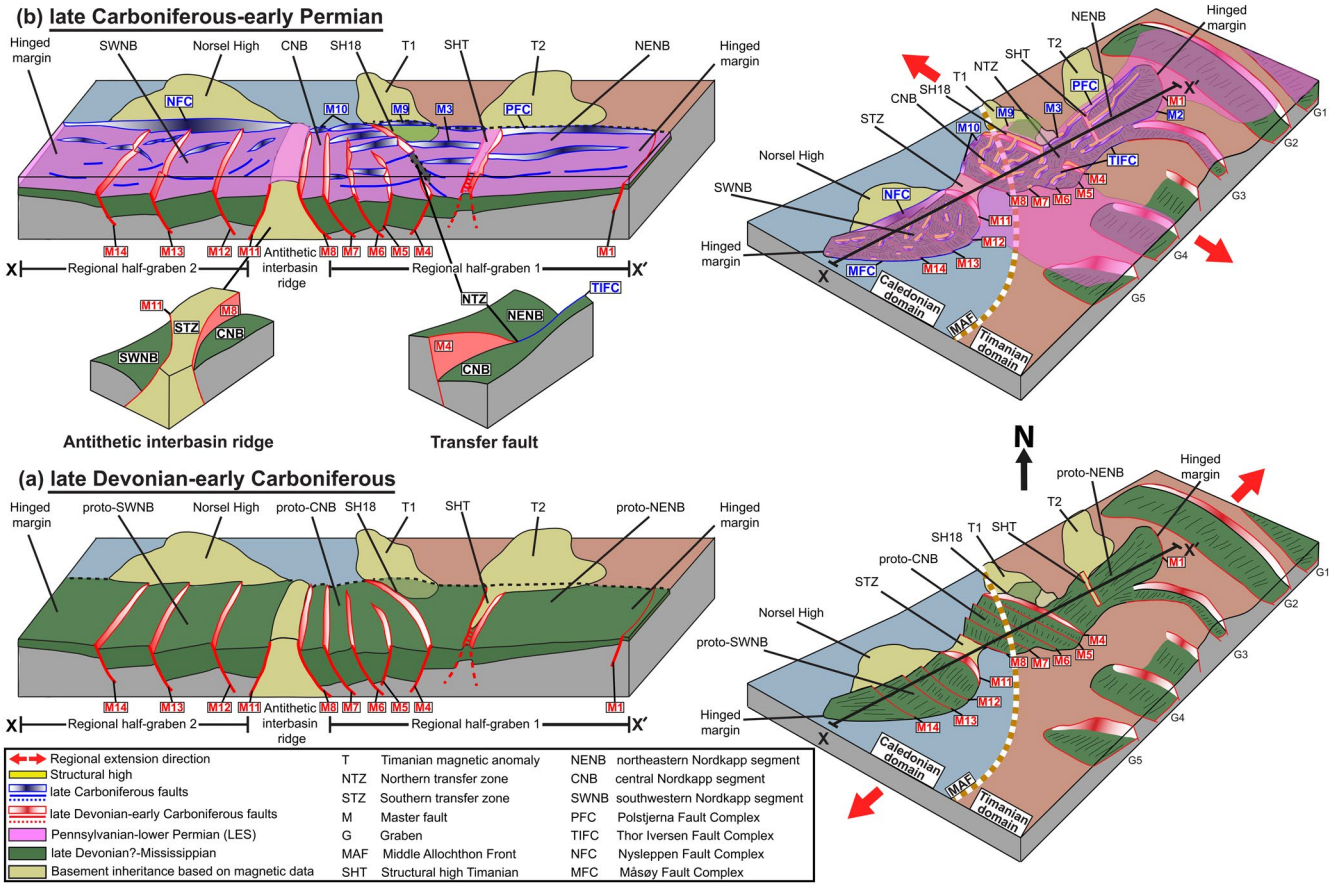

FIGURE 12 Conceptual structural evolution model for the Nordkapp Basin. (a) Late Devonian-early Carboniferous extension controlled mainly by NW-SE striking faults following the Timanian inherited structures. (b) Late Carboniferous-early Permian(?) extension controlled by NE-SW trending faults and the inherited structures [Colour figure can be viewed at wileyonlinelibrary.com]

lineations to the curvilinear Caledonian nappes fit with the internal subdivision of the SWNB segment. However, the influence of these lineations across the Norsel High region can be ruled out due to the presence of the deep Palaeozoic high (Figure 11).

5.2 | Basin architecture and segmentation

5.2.1 | Late Devonian-early Carboniferous extension

The magnetic data illustrate the complexity of basement topography, suggesting variable crustal thickness beneath the Nordkapp Basin. We suggest that this affected the Nordkapp Basin initiation and development during the two subsequent events of NE-SW and NW-SE oriented extension (Figure 12). Both the greater Barents Sea and the Timan-Pechora Basin (Figure 1a inset) were affected by a NE-SW oriented extension, which was oriented orthogonal to the trend of deep Timanian structures in the middle-late Devonian (Faleide et al., 2018; Hassaan et al., 2020; Klitzke et al., 2019; Stoupakova et al., 2011 and references therein). During the late Devonian-early Carboniferous NE-SW oriented extensional phase, the Nordkapp Basin comprised two regional half-grabens (Figure 12a). The proto-NENB and proto-CNB segments were parts of the regional half-graben-1, whereas the proto-SWNB segment belonged to the regional half-graben-2 that was separated from half-graben-1 by a prominent antithetic ridge, (Figures 5b, 6c and 12a; Hassaan et al., 2020). This is the main reason that the CNB segment is deeper than the NENB segment. A further subdivision within the regional half-graben-1 is created by the two structural highs, SH18 and SHT (Figures 6c and 12a). The magnetic data support this hypothesis and signify the control of the Timanian inherited structures as the SH18 developed on the southern edge of the deep structure (T1 magnetic anomaly), and the SHT seems to be part of the lineament related to the T2 magnetic anomaly (Figure 11b). To the north, the structural high SH18 also bounds the shallow outlier sub-basin SB4 that evolved over the deep Timanian structure (Figures 6c, 11b and 12a). The effect of the deep structures is maximum within the CNB segment, where the MAF

separates the Timanian and Caledonian domains within the Nordkapp Basin (Figure 11b). Although a significant part of the CNB segment has evolved over the Caledonian domain, the NW-SE striking normal faults have overprinted the pre-existing structural lineaments and signify the control of the late Devonian-early Carboniferous extension phase.

The 'antithetic interbasin ridge' acted as an interbasin transfer zone (sensu Gawthorpe & Hurst, 1993; named southern transfer zone, STZ). The STZ was formed due to the change in dip direction of the bounding faults M8 and M11 (Figures 5b, 6c and 11a). In contrast to the major tilted fault-blocks bounded by the NW-SE trending normal faults, the STZ is a relatively high-relief region (Figure 12a; Ebinger et al., 1987; Gawthorpe & Hurst, 1993; Rosendahl, 1987; Rosendahl et al., 1986). We suggest that the STZ was a pronounced feature during early Carboniferous due to the nonoverstepping of the two adjacent master faults M8 and M11, whilst it was subsequently covered by the later LES accumulation and postsalt sedimentation. Internally, the regional half-graben-2 was influenced by the NW-SE oriented M12–14 normal faults that were terminated against the Norsel High (Figures 6c and 12a). The Norsel High is a pronounced structural high at early Carboniferous level, formed due to the Caledonian orogen collapse and is probably underlain by crystalline Caledonian rocks (Gernigon et al., 2018 and references therein). The presence of the NW-SE trending faults highlights the dominant influence of the Timanian inherited structures on the NE-SW oriented regional extension within the Caledonian domain (Figures 11 and 12a). The M12–14 faults not only influenced the accumulation of the later LES within the depocenters but localised the subsequent scattered SS14–30 salt structures within the elongated SWNB segment in contrast to NENB segment (Figures 5, 6c and 11).

5.2.2 | Late Carboniferous extension

The extensional stress regime shifted to NW-SE orientation during the late Carboniferous and probably reactivated the NE-SW trending deeper inherited structures that controlled the evolution of the southwestern Barents Sea (Faleide et al., 2018; Gernigon et al., 2018; Gudlaugsson et al., 1998 and references therein). The region was under warm, arid to semi-arid climate conditions due to the drift into the subtropical zone, and as a consequence, the deposition of the warm-water carbonates and sabkha evaporites of the Gipsdalen Group (Figure 3) took place (Larssen et al., 2002; Stemmerik, 2000). The effect of the younger extension was less pronounced in the southeastern Norwegian Barents Sea, and layered evaporites within the Gipsdalen Group strata (Figure 3) were accumulated in postrift conditions (Figure 12b; Hassaan et al., 2020, 2021; Rowan & Lindsø, 2017). The NW-SE oriented extensional stress regime (Figure 12b) affected the regional NW-SE trending half-grabens within the proto-Nordkapp Basin (Figure 12a). Thus, the synrift to early postrift processes influenced the nature and thickness of the Pennsylvanian-lower Permian LES accumulated in the different incipient segments within the Nordkapp Basin (Figures 5b, 6c and 12b; Rowan & Lindsø, 2017). The Caledonian basement inheritance continued to play a vital role in the reactivation of the NE-SW oriented deeper structures that cross-cut the pre-existing NW-SE oriented structures in the two regional half-grabens (Figure 12b), together with the formation of late Palaeozoic basins in the southwestern Barents Sea (Figure 11b, blue stippled lines). Towards the hinged-margin of the regional half-graben-1, the thick-skinned Thor Iversen and Polstjerna fault complexes were reactivated (Figure 8b). The fault throw of theThor Iversen Fault Complex diminish towards the hinged-margin, probably due to the presence of the deep Timanian structure (Figure 8). Farther southwest of the SHT, the graben polarity changes due to reactivation of the Thor Iversen Fault Complex. We suggest that this is due to the termination of the thick and mechanically strong crust related to the CBSM magnetic anomaly outside the hinged-margin of the regional half-graben-1 (Figures 8b and 12b). The estimate of the evacuated salt thickness in the NENB segment (SB1: ca. 2.3 km and SB2: ca. 4.4 km, Table 4) suggests that the SB1 subbasin was a hinged-margin of the regional half-graben-1 (Figure 5b). The SHT structural high created the primary division between subbasins SB1 and SB2 and influenced the LES accumulation. However, towards the southwest of the SHT structural high, the subbasin SB2 induced a deeper and structurally active transitional region that trapped a thicker LES and became the site for complex salt structures (Figures 5b, 6c, 8b and 12b; Table 4).

The complex intersection between the Thor Inversen Fault Complex and master fault M4 with opposing polarity at the suggested boundary between the CNB and NENB segments has created a prominent transfer fault that acted as an interbasin transfer zone (sensu Gawthorpe & Hurst, 1993; named northern transfer zone, NTZ; Figures 6c and 12b). In the Nordkapp Basin, the transfer zone was formed during the late Carboniferous extension and separated the hinged-margin (proto-NENB) from the deeper part (proto-CNB) of the regional half-graben-1 (Figures 6c and 12b). The highly deformed region southwest of the SHT structural high could be related to the development of the northern transfer zone NTZ that has a character of thick-skinned reverse fault (Figures 6c and 8b, red arrow).

In the deeper region of the regional half-graben-1, the Thor Iversen Fault Complex and the M10 boundary fault were active and caused a series of fault-bounded structural highs (SH13-19) and gave rise to the development of the deeper subbasin SB3 into a full-graben. The structural highs SH13-19 overprinted the earlier NW-SE oriented faults M5-7 (Figures 6c and 12b). In subbasin SB4, the M9 boundary fault was active but did not cut through the strong structural high SH18, preventing it from merging with subbasin SB3. This is the main reason why subbasin SB4 remained an isolated shallow basin with less accumulation space for the LES (Figures 5b, 11 and 12b). Subbasin SB3 contains ca. 20,267 km^3 of mobile salt that is even larger than the cumulative salt volume in all other subbasins (Table 4). This suggests that subbasin SB3 was the most extended region evolving over the transitional crust that was formed due to the interaction between the Timanian and Caledonian inherited structures. The evacuated salt thickness of subbasins SB2 and SB3 is almost similar, and we suggest that subbasin SB2 was part of the more extensive rift system. Internally, subbasin SB3 contains isolated depocenters with spatially variable LES thicknesses that influenced the evolution of the salt structures (Figure 6a). In particular, the different segments of the composite DF salt structure were sourced by salt from multiple depocenters filled with LES (Figures 5 and 6a; Hassaan et al., 2021).

The regional half-grabens-1 and 2 were separated from each other by the STZ transfer zone. During the late Carboniferous extension, the basin boundary between the Nysleppen and Måsøy fault complexes was activated and led to further subsidence within the regional half-graben-2 (Figure 10). The Nysleppen Fault Complex was more active as a boundary due to its location between the regional half-graben-2 and the Norsel High (Figures 10 and 12b). Overall, the LES as graben infill was thickening towards the Nysleppen Fault Complex, whilst the NW-SE striking M12-14 faults compartmentalised the regional half-graben-2 (Figures 5b, 6c and 10). The cross-cutting faults led to the development of scattered fault-bounded structural highs at the end of the late Carboniferous extension. We suggest that the SH21-37 structural highs were strongly influenced by the NW-SE striking M12-14 faults and have played an important role during the accumulation of the Pennsylvanian-lower Permian LES. The SWNB segment contains the smallest volume of evacuated salt (ca. 6,192 km^3) in the Nordkapp Basin (Table 3). However, the base of the LES in the SWNB segment is deep, that is, ca. 5- to 6-s twt, and apparently, the nonmobile LES are thickest there in comparison to the NENB and CNB segments (Figures 5b,c and 8–10; Table 3). We suggest that the eroded sediments from the Norsel High contaminated the LES during late Carboniferous to early Permian and affected the LES nature from mobile to nonmobile (Figure 5b,c).

5.3 | Presalt basin architecture and LES: A substratum to impact the subsequent basin evolution

The presalt basement topography likely had an indirect but profound impact on the primary distribution of postsalt sediments. This would, however, also be influenced by the primary qualities of evaporites, like viscosity and palaeotemperature (Allen & Beaumont, 2016; Hudec et al., 2009). The sediment stratigraphy (layering) is likely to influence the relative viscosity of the salt within the LES so it can be speculated that the effective viscosity may be different from that of the single-layer salt system (Rowan et al., 2019 and references therein). We consider it may be likely that the LES in the Nordkapp Basin has relatively low viscosity, and consequently, the presalt basin architecture may strongly influence the sediment routing and depositional fairways for postsalt sediments (Hassaan et al., in review). During the early to late Permian, the depositional environment shifted to temperate conditions and allowed the deposition of cool-water carbonate platforms of the Bjarmeland and Tempelfjorden groups (Figure 3; Beauchamp, 1994; Stemmerik, 2000). We suggest two possible scenarios at the end of the accumulation of the Pennsylvanian-lower Permian synrift to early postrift LES and the late Permian formation of carbonate platforms (Figure 13). In the first scenario, the basin topography was not smooth due to the preceding extension and it possessed some relief mimicking the underlying rift architecture (Figure 13b–e). In this case, the residual topographic expression will, in turn, influence the earliest Triassic progradational sediment routings and dictate both where the initial deposition could take place and the formation of distinct depositional fairways (Hassaan et al., in review). In the second scenario, the basin topography was levelled and smoothed out the residual top-rift topography (Figure 13b–e). However, the base of the LES retained the rift architecture configuration and the thickness of the accumulated Pennsylvanian-lower Permian LES varies spatially in the different subbasins of the Nordkapp Basin. Nevertheless, the progradational system arriving in Nordkapp Basin from the east would respond to the deep rift architecture due to the presence of the thick mobile LES units within it during the earliest Triassic. This is due to the creation of the drastic lateral differential load gradient due to postsalt progradational sediment load and scattered presalt Carboniferous structural highs (SH1-37) that provided the basis for the location of the salt structures in both scenarios (Figure 5).

The postsalt Triassic depositional fairways would have several effects on the surrounding sedimentary system in the minibasins (Hassaan et al., in review). These may include the bypass of some areas with thicker salt, that is, even areas with thick salt in the LES may not record any sedimentary successions and the inhibition of sedimentation adjacent to the depositional

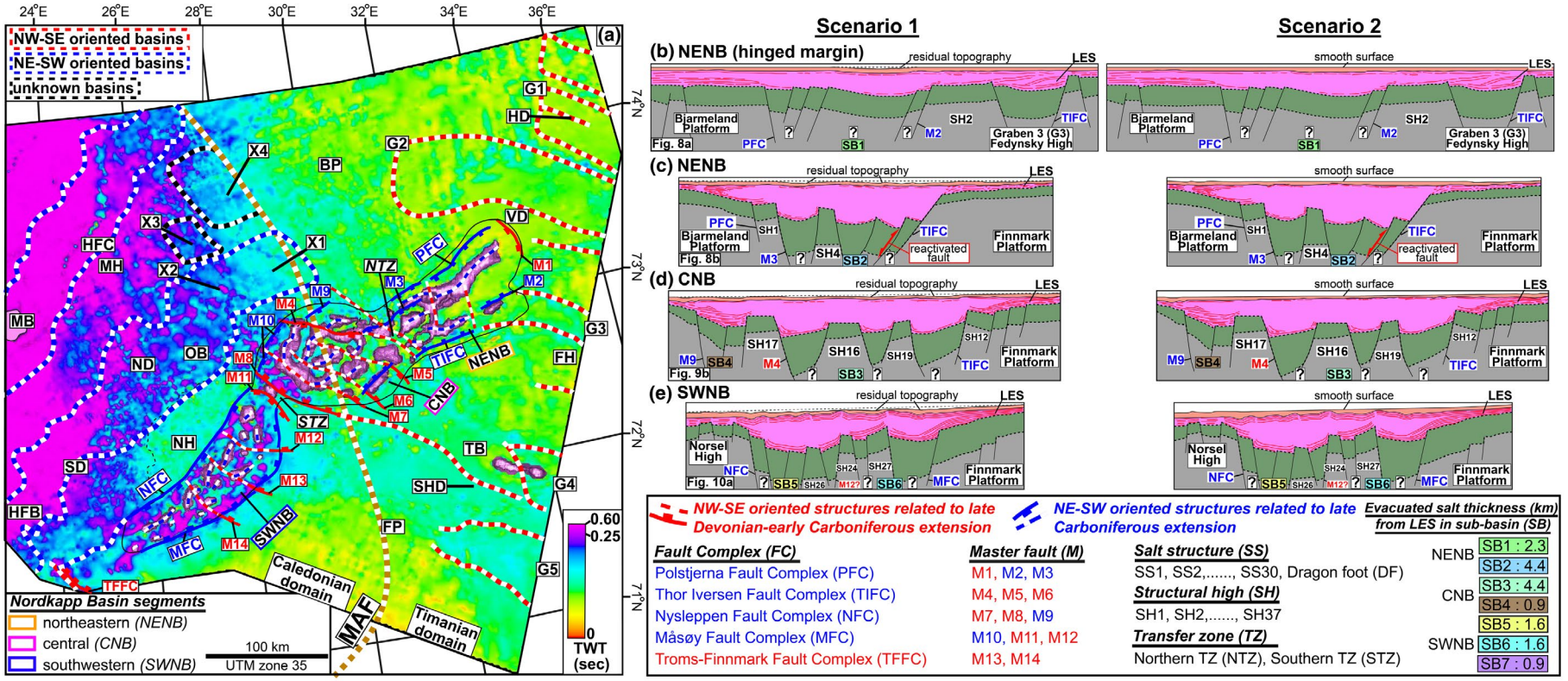

FIGURE 13 (a) Regional thickness map (TWT: two-way travel time, s) of the upper Permian sequence S0 overlaid with the structural configuration based on seismic interpretation in the southeastern and southwestern Barents Sea. X1-4: newly interpreted/inferred basins (see text for details). (b–e) The restored models display two possible scenarios related to residual topography and smooth surface by the end of upper Permian sequence S0 accumulation (Hassaan et al., in review). Note the reactivated normal fault in contrast to present-day reverse fault in Figure 8b. The utilised abbreviations (followed by number or letter) denote: BP: Bjarmeland Platform; FH: Fedynsky High; FP: Finnmark Platform; G: Graben; MAF: Middle Allochthon Front; NH: Norsel High; TB: Tiddlybanken Basin; VD: Veslekari Dome. Other abbreviations as in Figure 1a [Colour figure can be viewed at wileyonlinelibrary.com]

fairway. The depositional fairways primarily formed by differential loading and density-driven subsidence caused by the progradational sedimentation and have restricted the subsidence in the mini-basins outside the fairways (Fernandez et al., 2020). Therefore, the accumulated LES together with the presalt rift architecture comprised a laterally varying in thickness and physical properties substratum that during the earliest Triassic influenced the progradational sediment routings and deposition. Furthermore, the discrepancies both in the present-day cumulative salt volume in the main NENB, CNB and SWNB segments (Table 3) and in the estimated average evacuated salt thickness in the various subbasins SB1–SB7 (Table 4) are indirect indications of the presalt rift architecture variability within the Nordkapp Basin (Figures 5b and 6). This is likely the main reason that the LES substratum in subbasins SB2 and SB3 was more prone to salt mobilisation than in the other subbasins and has created greater accommodation space for postsalt sediments (Figures 8–10). We suggest that the temporarily and drastically localised sedimentation above a portion of the underlying structures would not be possible without thick LES that is indirectly a consequence of the presalt rift architecture. In this context, the direction and how fast the prograding system will fill the depositional fairway over the LES and the presalt rift architecture are also essential (Hassaan et al., in review). Similarly, as for the Tiddlybanken Basin and southwestern Barents Sea area in the nearby vicinity, Carboniferous structures in the Nordkapp Basin were also reactivated by far-field stresses propagating both during late Triassic due to the evolving Novaya Zemlya fold-and-thrust belt farther to the east and during early-middle Eocene as a result of the transpressional Eurekan/Spitsbergen orogeny farther to the northwest (e.g. Figure 8b; Gac et al., 2020; Hassaan et al., 2020, 2021). We suggest that during these far-field compressional events, the salt structures underlain by the basement-involved structural highs within the Nordkapp Basin were more rejuvenated due to stress propagation in contrast to the saddle areas where the master faults cross-cut, particularly within the CNB segment (Figures 5b,c and 6c).

6 | CONCLUSIONS

We utilised reprocessed regional 2D seismic reflection profiles, 3D seismic data, available wells and magnetic and gravity data to study the salt-influenced Nordkapp Basin in the Barents Sea. The Nordkapp Basin can be subdivided into three main segments (northeastern, central, and southwestern). It evolved above a pre-Carboniferous basement that includes remnants of the Timanian and Caledonian orogenies. The curvilinear magnetic lineations of the Caledonian structures pass through the central segment, where the Middle Allochthonous Front (an amalgamation of thrust units) creates the major subdivision between the Timanian and Caledonian inherited structures. We suggest that the rheological properties of the Timanian and Caledonian inherited structures, together with their regional distribution, orientation and spatial interaction in combination with two subsequent regional extensional phases, have strongly influenced the presalt rift architecture and gave rise to seven subbasins within the Nordkapp Basin.

During late Devonian-early Carboniferous, a NE-SW oriented extensional phase took place and the three Nordkapp Basin segments were parts of two NW-SE oriented regional half-grabens (northern and southern) separated by a prominent interbasin ridge. During the late Carboniferous-early Permian(?), a second extensional phase took place and the stress orientation shifted to NW-SE and influenced the configuration of the regional half-grabens. A transfer fault divided the northern regional half-graben by separating its hinged-margin from the deeper part and developed the incipient northeastern and central Nordkapp Basin segments, respectively. At the same time, the prominent interbasin ridge acted as a transfer zone and created a partition between the central and southwestern segments of the Nordkapp Basin. The Thor Iversen, Polstjerna, Måsøy and Nysleppen basin boundary fault complexes were formed during this process. Internally, the seven subbasins were affected by the cross-cutting master faults and structural highs that controlled the accumulation of the Pennsylvanian-lower Permian LES and the subsequent formation and location of the salt structures. The synrift to early postrift processes, relative depth of each subbasin, the internal arrangement of the structural highs and the depositional palaeo-environment, all controlled the thickness and facies of the LES. The spatially variable LES substratum impacted the postsalt evolution as the subbasins with thicker LES were more prone to salt mobilisation. We suggest that during the earliest Triassic, the top of the basin topography was an irregular surface inherited from the preceding extension episodes and possessed distinct relief mimicking the underlying rift architecture. The residual topography influenced, in turn, the progradational sediment routings and dictated where the initial deposition could take place. In this context, the direction and how fast the accumulated prograding system arriving from the east will fill the initial depocenters over the LES would define the postsalt sedimentary evolution within the Nordkapp Basin.

The current study highlights the significance of the complex presalt rift architecture in a salt-influenced rift basin and the consequent implications for the synrift to early postrift LES accumulation, location of salt structures and postsalt sedimentary evolution. The analysis has revealed in detail the presalt rift architecture and the processes that impacted the upper Palaeozoic evolution of the Nordkapp

Basin that is the largest salt basin in Barents Sea and could be applicable to the study of other salt-influenced rift basins worldwide.

ACKNOWLEDGEMENTS

The study is part of the ARCEx (Research Centre for Arctic Petroleum Exploration) project which is funded by the Research Council of Norway (grant number 228107) together with 10 academic and 6 industry (Equinor, Vår Energi, AkerBP, Lundin Energy Norway, OMV and Wintershall Dea) partners. We want to thank all academic institutes, industry and funding partners. Vår Energi is acknowledged for sponsoring the Adjunct Professor position of F. Tsikalas at the University of Oslo. Reviews by Jafar Hassanpour and Oliver B. Duffy, with editorial remarks from Craig Magee, helped to improve the manuscript. Schlumberger and Petroleum Experts are thanked for providing academic licences to the Petrel© and Move© software, respectively. The Norwegian Petroleum Directorate (NPD) and TGS-NOPEC Geophysical Company ASA are also acknowledged for providing access to the regional 2D seismic and 3D seismic data. The technical contents and ideas presented herein are solely the authors' interpretations.

CONFLICT OF INTEREST

The authors declare that they have no conflict of interest.

AUTHORS CONTRIBUTIONS

M.H. and J.I.F designed and directed the research. M.H. interpreted the magnetic, gravity and seismic data. M.H., J.I.F., R.H.G. and F.T. analysed the results and contributed to interpretation of the same. M.H. prepared the figures and wrote the manuscript text. All authors edited the manuscript.

PEER REVIEW

The peer review history for this article is available at https://publons.com/publon/10.1111/bre.12565.

DATA AVAILABILITY STATEMENT

The data that support the findings of this study are available from NPD and TGS. Restrictions apply to the availability of these data, which were used under licence for this study.

ORCID

Muhammad Hassaan https://orcid.org/0000-0001-6004-8557

REFERENCES

Allen, J., & Beaumont, C. (2016). Continental margin syn-rift salt tectonics at intermediate width margins. *Basin Research*, *28*(5), 598–633. https://doi.org/10.1111/bre.12123

Baig, I., Faleide, J. I., Jahren, J., & Mondol, N. H. (2016). Cenozoic exhumation on the southwestern Barents Shelf: Estimates and uncertainties constrained from compaction and thermal maturity analyses. *Marine and Petroleum Geology*, *73*, 105–130. https://doi.org/10.1016/j.marpetgeo.2016.02.024

Barrère, C., Ebbing, J., & Gernigon, L. (2009). Offshore prolongation of Caledonian structures and basement characterisation in the western Barents Sea from geophysical modelling. *Tectonophysics*, *470*(1–2), 71–88. https://doi.org/10.1016/j.tecto.2008.07.012

Barrère, C., Ebbing, J., & Gernigon, L. (2011). 3-D density and magnetic crustal characterization of the southwestern Barents Shelf: Implications for the offshore prolongation of the Norwegian Caledonides. *Geophysical Journal International*, *184*(3), 1147–1166. https://doi.org/10.1111/j.1365-246X.2010.04888.x

Beauchamp, B. (1994). Permian climatic cooling in the Canadian Arctic. *Geological Society of America Special Paper*, *288*, 229–246.

Breivik, A. J., Gudlaugsson, S. T., & Faleide, J. I. (1995). Ottar Basin, SW Barents Sea: A major Upper Palaeozoic rift basin containing large volumes of deeply buried salt. *Basin Research*, *7*, 299–312. https://doi.org/10.1111/j.1365-2117.1995.tb00119.x

Bugge, T., Mangerud, G., Elvebakk, G., Mørk, A., Nilsson, I., Fanavoll, S., & Vigran, J. O. (1995). The upper palaeozoic succession on the Finnmark platform, Barents Sea. *Norsk Geologisk Tidsskrift*, *75*(1), 3–30.

Cedeño, A., Rojo, L. A., Cardozo, N., Centeno, L., & Escalona, A. (2019). The impact of salt tectonics on the thermal evolution and the petroleum system of confined rift basins: insights from basin modeling of the Nordkapp Basin, Norwegian Barents Sea. *Geosciences*, *9*(7), 316. https://doi.org/10.3390/geosciences9070316

Dengo, C. A., & Røssland, K. G. (1992). Extensional tectonic history of the western Barents Sea. In R. M. Larsen, H. Brekke, B. T. Larsen & E. Talleraas (Eds.), *Structural and tectonic modelling and its application to petroleum geology* (pp. 91–107). Oslo, Norway: Norwegian Petroleum Society Special Publication 1. https://doi.org/10.1016/B978-0-444-88607-1.50011-5

Ebinger, C. J., Rosendahl, B., & Reynolds, D. (1987). Tectonic model of the Malaŵi rift, Africa. *Tectonophysics*, *141*(1–3), 215–235. https://doi.org/10.1016/0040-1951(87)90187-9

Eide, C. H., Klausen, T. G., Katkov, D., Suslova, A. A., & Helland-Hansen, W. (2018). Linking an Early Triassic delta to antecedent topography: Source-to-sink study of the southwestern Barents Sea margin. *GSA Bulletin*, *130*(1–2), 263–283. https://doi.org/10.1130/B31639.1

Faleide, J. I., Pease, V., Curtis, M., Klitzke, P., Minakov, A., Scheck-Wenderoth, M., Kostyuchenko, S., & Zayonchek, A. (2018). Tectonic implications of the lithospheric structure across the Barents and Kara shelves. *Geological Society, London, Special Publications*, *460*(1), 285–314. https://doi.org/10.1144/SP460.18

Faleide, J. I., Tsikalas, F., Breivik, A. J., Mjelde, R., Ritzmann, O., Engen, Ø., Wilson, J., & Eldholm, O. (2008). Structure and evolution of the continental margin off Norway and the Barents Sea. *Episodes*, *31*(1), 82–91. https://doi.org/10.18814/epiiugs/2008/v31i1/012

Faleide, J. I., Vågnes, E., & Gudlaugsson, S. T. (1993). Late Mesozoic-Cenozoic evolution of the south-western Barents Sea in a regional rift-shear tectonic setting. *Marine and Petroleum Geology*, *10*(3), 186–214. https://doi.org/10.1016/0264-8172(93)90104-Z

Fernandez, N., Hudec, M. R., Jackson, C.-A.-L., Dooley, T. P., & Duffy, O. B. (2020). The competition for salt and kinematic interactions between minibasins during density-driven subsidence: Observations from numerical models. *Petroleum Geoscience*, *26*(1), 3–15. https://doi.org/10.1144/petgeo2019-051

Gabrielsen, R. (1984). Long-lived fault zones and their influence on the tectonic development of the southwestern Barents Sea. *Journal of the Geological Society*, *141*(4), 651–662. https://doi.org/10.1144/gsjgs.141.4.0651

Gabrielsen, R. H., Faerseth, R. B., & Jensen, L. N. (1990). *Structural elements of the Norwegian Continental Shelf. Pt. 1. The Barents Sea Region*. Norwegian Petroleum Directorate.

Gabrielsen, R. H., Grunnaleite, I., & Rasmussen, E. (1997). Cretaceous and tertiary inversion in the Bjørnøyrenna Fault Complex, southwestern Barents Sea. *Marine and Petroleum Geology*, *14*, 165–178. https://doi.org/10.1016/S0264-8172(96)00064-5

Gac, S., Minakov, A., Shephard, G. E., Faleide, J. I., & Planke, S. (2020). Deformation analysis in the Barents Sea in relation to Paleogene transpression along the Greenland-Eurasia plate boundary. *Tectonics*, *39*, 6172. https://doi.org/10.1029/2020TC006172

Gawthorpe, R., & Hurst, J. M. (1993). Transfer zones in extensional basins: Their structural style and influence on drainage development and stratigraphy. *Journal of the Geological Society*, *150*(6), 1137–1152. https://doi.org/10.1144/gsjgs.150.6.1137

Gee, D., Bogolepova, O., & Lorenz, H. (2006). The Timanide, Caledonide and Uralide orogens in the Eurasian high Arctic, and relationships to the palaeo-continents Laurentia, Baltica and Siberia. *Geological Society, London, Memoirs*, *32*(1), 507–520. https://doi.org/10.1144/GSL.MEM.2006.032.01.31

Gernigon, L., & Brönner, M. (2012). Late Palaeozoic architecture and evolution of the southwestern Barents Sea: Insights from a new generation of aeromagnetic data. *Journal of the Geological Society*, *169*(4), 449–459. https://doi.org/10.1144/0016-76492011-131

Gernigon, L., Brönner, M., Dumais, M.-A., Gradmann, S., Grønlie, A., Nasuti, A., & Roberts, D. (2018). Basement inheritance and salt structures in the SE Barents Sea: Insights from new potential field data. *Journal of Geodynamics*, *119*, 82–106. https://doi.org/10.1016/j.jog.2018.03.008

Gernigon, L., Brönner, M., Roberts, D., Olesen, O., Nasuti, A., & Yamasaki, T. (2014). Crustal and basin evolution of the southwestern Barents Sea: From Caledonian orogeny to continental breakup. *Tectonics*, *33*(4), 347–373. https://doi.org/10.1002/2013TC003439

Glørstad-Clark, E., Faleide, J. I., Lundschien, B. A., & Nystuen, J. P. (2010). Triassic seismic sequence stratigraphy and paleogeography of the western Barents Sea area. *Marine and Petroleum Geology*, *27*(7), 1448–1475. https://doi.org/10.1016/j.marpetgeo.2010.02.008

Gradstein, F. M., & Ogg, J. G. (2020). The chronostratigraphic scale. In *Geologic Time Scale 2020* (pp. 21–32). Elsevier. https://doi.org/10.1016/B978-0-12-824360-2.00002-4.

Grimstad, S. (2016). Salt tectonics in the central and northeastern Nordkapp Basin, Barents Sea. Master Thesis, University of Oslo, Norway, 1–127.

Gudlaugsson, S., Faleide, J., Johansen, S., & Breivik, A. (1998). Late Palaeozoic structural development of the south-western Barents Sea. *Marine and Petroleum Geology*, *15*(1), 73–102. https://doi.org/10.1016/S0264-8172(97)00048-2

Hassaan, M., Faleide, J. I., Gabrielsen, R. H., & Tsikalas, F. (2020). Carboniferous graben structures, evaporite accumulations and tectonic inversion in the southeastern Norwegian Barents Sea. *Marine and Petroleum Geology*, *112*, 104038. https://doi.org/10.1016/j.marpetgeo.2019.104038

Hassaan, M., Faleide, J. I., Gabrielsen, R. H., & Tsikalas, F. (2021). Architecture of the evaporite accumulation and salt structures dynamics in Tiddlybanken Basin, southeastern Norwegian Barents Sea. *Basin Research*, *33*(1), 91–117. https://doi.org/10.1111/bre.12456

Hassaan, M., Faleide, J. I., Gabrielsen, R. H., Tsikalas, F., & Grimstad, S. (in review). Interplay between base-salt relief, progradational sediment loading and salt tectonics in the Nordkapp basin, Barents Sea–Part II.

Henriksen, E., Bjørnseth, H., Hals, T., Heide, T., Kiryukhina, T., Kløvjan, O., & Sollid, K. (2011). Uplift and erosion of the greater Barents Sea: Impact on prospectivity and petroleum systems. *Geological Society, London, Memoirs*, *35*(1), 271–281.

Hudec, M. R., Jackson, M. P., & Schultz-Ela, D. D. (2009). The paradox of minibasin subsidence into salt: Clues to the evolution of crustal basins. *Geological Society of America Bulletin*, *121*(1–2), 201–221.

Indrevær, K., Gac, S., Gabrielsen, R. H., & Faleide, J. I. (2018). Crustal-scale subsidence and uplift caused by metamorphic phase changes in the lower crust: A model for the evolution of the Loppa High area, SW Barents Sea from late Paleozoic to Present. *Journal of the Geological Society*, *175*(3), 497–508. https://doi.org/10.1144/jgs2017-063

Jensen, L. N., & Sørensen, K. (1992). Tectonic framework and halokinesis of the Nordkapp Basin, Barents Sea. In R. M. Larsen, H. Brekke, B. T. Larsen, & E. Talleraas, *Structural and tectonic modelling and its application to petroleum geology* (pp. 109–120). Oslo, Norway, Norwegian: Petroleum Society Special Publication 1. https://doi.org/10.1016/B978-0-444-88607-1.50012-7

Klausen, T. G., Ryseth, A. E., Helland-Hansen, W., Gawthorpe, R., & Laursen, I. (2015). Regional development and sequence stratigraphy of the Middle to Late Triassic Snadd formation, Norwegian Barents Sea. *Marine and Petroleum Geology*, *62*, 102–122. https://doi.org/10.1016/j.marpetgeo.2015.02.004

Klitzke, P., Franke, D., Ehrhardt, A., Lutz, R., Reinhardt, L., Heyde, I., & Faleide, J. (2019). The Paleozoic evolution of the Olga Basin region, northern Barents Sea–A link to the Timanian Orogeny. *Geochemistry, Geophysics, Geosystems*, *20*(2), 614–629. https://doi.org/10.1029/2018GC007814

Koyi, H., Talbot, C. J., & Tørudbakken, B. O. (1993). Salt diapirs of the southwest Nordkapp Basin: Analogue modelling. *Tectonophysics*, *228*(3–4), 167–187. https://doi.org/10.1016/0040-1951(93)90339-L

Koyi, H., Talbot, C. J., & Tørudbakken, B. O. (1995). Salt tectonics in the Northeastern Nordkapp Basin, Southwestern Barents sea. *AAPG Memoir*, *65*, 437–447.

Larssen, G., Elvebakk, G., Henriksen, L. B., Kristensen, S., Nilsson, I., Samuelsberg, T., & Worsley, D. (2002). Upper Palaeozoic lithostratigraphy of the Southern Norwegian Barents Sea. *Norwegian Petroleum Directorate Bulletin*, *9*, 76.

Lasabuda, A., Laberg, J. S., Knutsen, S.-M., & Høgseth, G. (2018). Early to middle Cenozoic paleoenvironment and erosion estimates of the southwestern Barents Sea: Insights from a regional mass-balance approach. *Marine and Petroleum Geology*, *96*, 501–521. https://doi.org/10.1016/j.marpetgeo.2018.05.039

Lasabuda, A., Laberg, J. S., Knutsen, S.-M., & Safronova, P. (2018). Cenozoic tectonostratigraphy and pre-glacial erosion: A mass-balance study of the northwestern Barents Sea margin, Norwegian Arctic. *Journal of Geodynamics*, *119*, 149–166. https://doi.org/10.1016/j.jog.2018.03.004

Marello, L., Ebbing, J., & Gernigon, L. (2013). Basement inhomogeneities and crustal setting in the Barents Sea from a combined 3D gravity and magnetic model. *Geophysical Journal International*, *193*(2), 557–584. https://doi.org/10.1093/gji/ggt018

Mattingsdal, R., Høy, T., Simonstad, E., & Brekke, H. (2015). *An updated map of structural elements in the southern Barents Sea*. Paper presented at the 31st Geological Winter Meeting

Midtkandal, I., Faleide, T. S., Faleide, J. I., Planke, S., Anell, I., & Nystuen, J. P. (2020). Nested intrashelf platform clinoforms—Evidence of shelf platform growth exemplified by Lower Cretaceous strata in the Barents Sea. *Basin Research*, *32*(2), 216–223. https://doi.org/10.1111/bre.1237

Müller, R., Klausen, T., Faleide, J., Olaussen, S., Eide, C., & Suslova, A. (2019). Linking regional unconformities in the Barents Sea to compression-induced forebulge uplift at the Triassic-Jurassic transition. *Tectonophysics*, *765*, 35–51. https://doi.org/10.1016/j.tecto.2019.04.006

Nilsen, K. T., Vendeville, B. C., & Johansen, J.-T. (1995). Influence of regional tectonics on halokinesis in the Nordkapp Basin, Barents Sea.

Pease, V., Scarrow, J., Silva, I. N., & Cambeses, A. (2016). Devonian magmatism in the Timan Range, Arctic Russia—Subduction, post-orogenic extension, or rifting? *Tectonophysics*, *691*, 185–197. https://doi.org/10.1016/j.tecto.2016.02.002

Rice, A., Gayer, R., Robinson, D., & Bevins, R. (1989). Strike-slip restoration of the Barents Sea Caledonides Terrane, Finnmark, north Norway. *Tectonics*, *8*(2), 247–264. https://doi.org/10.1029/TC008i002p00247

Ritzmann, O., & Faleide, J. I. (2007). Caledonian basement of the western Barents Sea. *Tectonics*, *26*(5). https://doi.org/10.1029/2006TC002059

Roberts, D. (1972). *Tectonic deformation in the Barents Sea region of Varanger peninsula, Finnmark*. Universitetsforlaget.

Roberts, D., & Gee, D. G. (1985). An introduction to the structure of the Scandinavian Caledonides. *The Caledonide Orogen–Scandinavia and Related Areas*, *1*, 55–68.

Rojo, L. A., Cardozo, N., Escalona, A., & Koyi, H. (2019). Structural style and evolution of the Nordkapp Basin, Norwegian Barents Sea. *AAPG Bulletin*, *103*(9), 2177–2217. https://doi.org/10.1306/01301918028

Rojo, L. A., & Escalona, A. (2018). Controls on minibasin infill in the Nordkapp Basin: Evidence of complex Triassic synsedimentary deposition influenced by salt tectonics. *AAPG Bulletin*, *102*(7), 1239–1272. https://doi.org/10.1306/0926171524316523

Rosendahl, B. R. (1987). Architecture of continental rifts with special reference to East africa. *Annual Review of Earth and Planetary Sciences*, *15*, 445. https://doi.org/10.1146/annurev.ea.15.050187.002305

Rosendahl, B., Reynolds, D., Lorber, P., Burgess, C., McGill, J., Scott, D., Lambiase, J., & Derksen, S. (1986). Structural expressions of rifting: Lessons from Lake Tanganyika, Africa. *Geological Society, London, Special Publications*, *25*(1), 29–43. https://doi.org/10.1144/GSL.SP.1986.025.01.04

Rowan, M. G., & Lindsø, S. (2017). Salt Tectonics of the Norwegian Barents sea and northeast Greenland shelf. In J. I. Soto, J. F. Flinch & G. Tari (Eds.), *Permo-Triassic Salt Provinces of Europe, North Africa and the Atlantic Margins* (pp. 265–286). London: Elsevier. https://doi.org/10.1016/B978-0-12-809417-4.00013-6

Rowan, M. G., Urai, J. L., Fiduk, J. C., & Kukla, P. A. (2019). Deformation of intrasalt competent layers in different modes of salt tectonics. *Solid Earth*, *10*(3), 987–1013. https://doi.org/10.5194/se-10-987-2019

Stemmerik, L. (2000). Late Palaeozoic evolution of the North Atlantic margin of Pangea. *Palaeogeography, Palaeoclimatology, Palaeoecology*, *161*(1–2), 95–126. https://doi.org/10.1016/S0031-0182(00)00119-X

Stoupakova, A., Henriksen, E., Burlin, Y. K., Larsen, G., Milne, J., Kiryukhina, T., Golynchik, P., Bordunov, S., Ogarkova, M., & Suslova, A. (2011). The geological evolution and hydrocarbon potential of the Barents and Kara shelves. *Geological Society, London, Memoirs*, *35*(1), 325–344.

Tsikalas, F., Blaich, O. A., Faleide, J. I., & Olaussen, S. (2021). Stappen High-Bjørnøya tectono-sedimentary element, Barents Sea. In S. S. Drachev, H. Brekke, E. Henriksen & T. Moore (Eds.), *Sedimentary successions of the Arctic Region and their hydrocarbon prospectivity*. Geological Society, London, Memoirs (Vol. *57*). https://doi.org/10.1144/M57-2016-24

Tsikalas, F., Faleide, J. I., Eldholm, O., & Blaich, O. A. (2012). The NE Atlantic conjugate margins. In D. G. Roberts, & A. W. Bally (Eds.), *Regional geology and tectonics: phanerozoic passive margins, Cratonic basins and global tectonic maps* (pp. 141–200). Elsevier.

How to cite this article: Hassaan M, Inge Faleide J, Helge Gabrielsen R, Tsikalas F. Effects of basement structures and Carboniferous basin configuration on evaporite distribution and the development of salt structures in Nordkapp Basin, Barents Sea—Part I. *Basin Res*. 2021;33:2474–2499. https://doi.org/10.1111/bre.12565